Intoduction to Normal mode theory and observation

John Woodhouse

Smolenice, September 2005

- A central goal of global seismology is to map the Earth's internal structure in three dimensions
- Imaging employs very large data sets of globally recorded seismograms
- Research aims to invent methods of analyzing seismic waveforms to maximize the retrieval of structural information and to use such information in large scale inverse problems

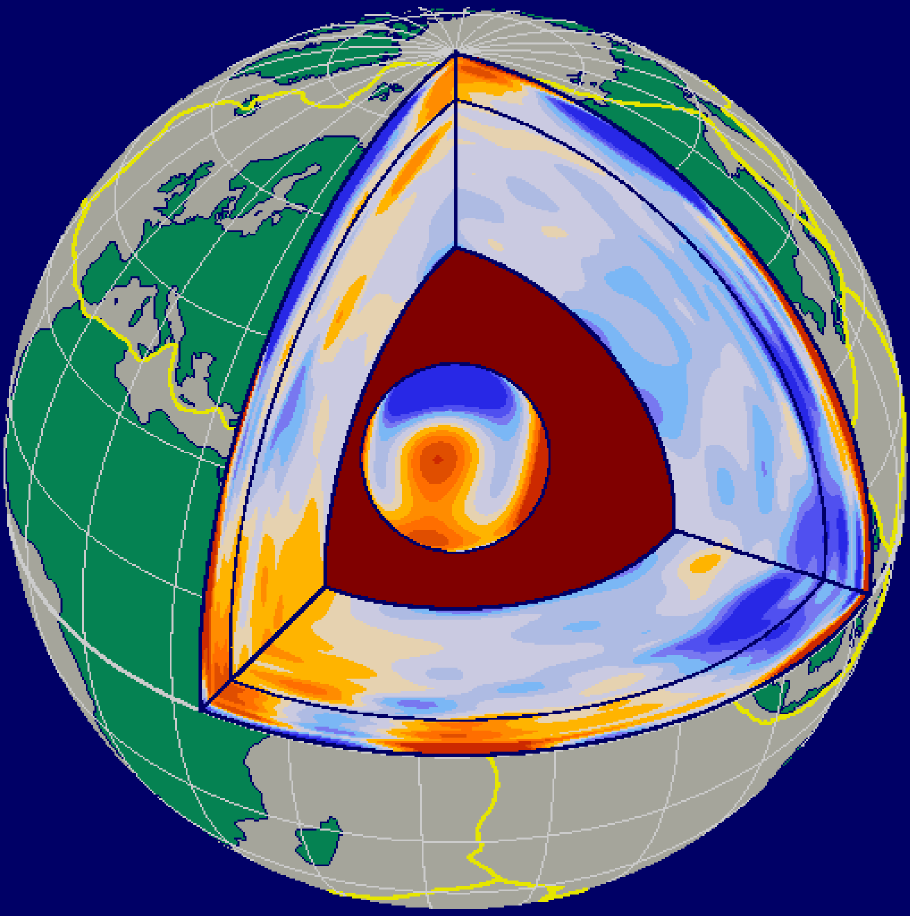

Model S20RTS: Ritsema, van Heijst and Woodhouse 1999,2004

Free Oscillations or Normal modes

The study of the Earth's Free Oscillations, or normal modes, can be regarded as

e) A useful way to calculate theoretical seismograms

g) As the intrinsic and observable spectrum of the Earth

The textbook picture:

P-waves

S-waves

Rayleigh waves

Love waves

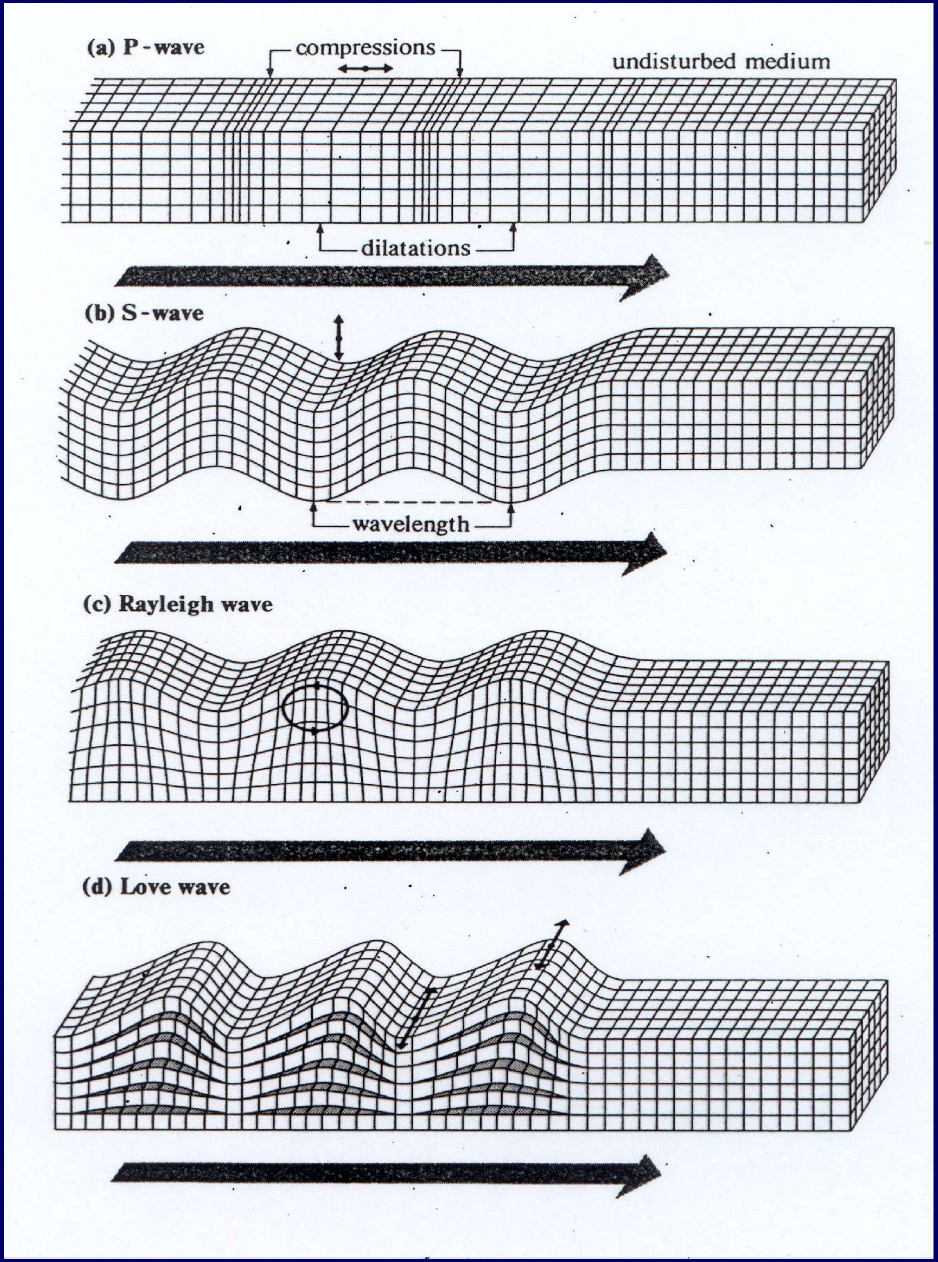

The Dispersion curve

$$\boxed{\omega = \omega(k)}$$

Where:
ω = Frequency (radians/second) = 2π/Period
k = Wave number (radians/km) = 2π/Wavelength

Then:
Phase velocity: $c = \omega/k = c(\omega)$ (km/s)
Group velocity: $U = d\omega/dk = U(\omega)$ (km/s)

In the laterally varying Earth, this translates into the concept of a ***local dispersion relation:***

$$\boxed{\omega = \omega(k,\theta,\varphi)}$$

Where θ,φ are colatitude and longitude.

The dispersion curve ω = ω(k)

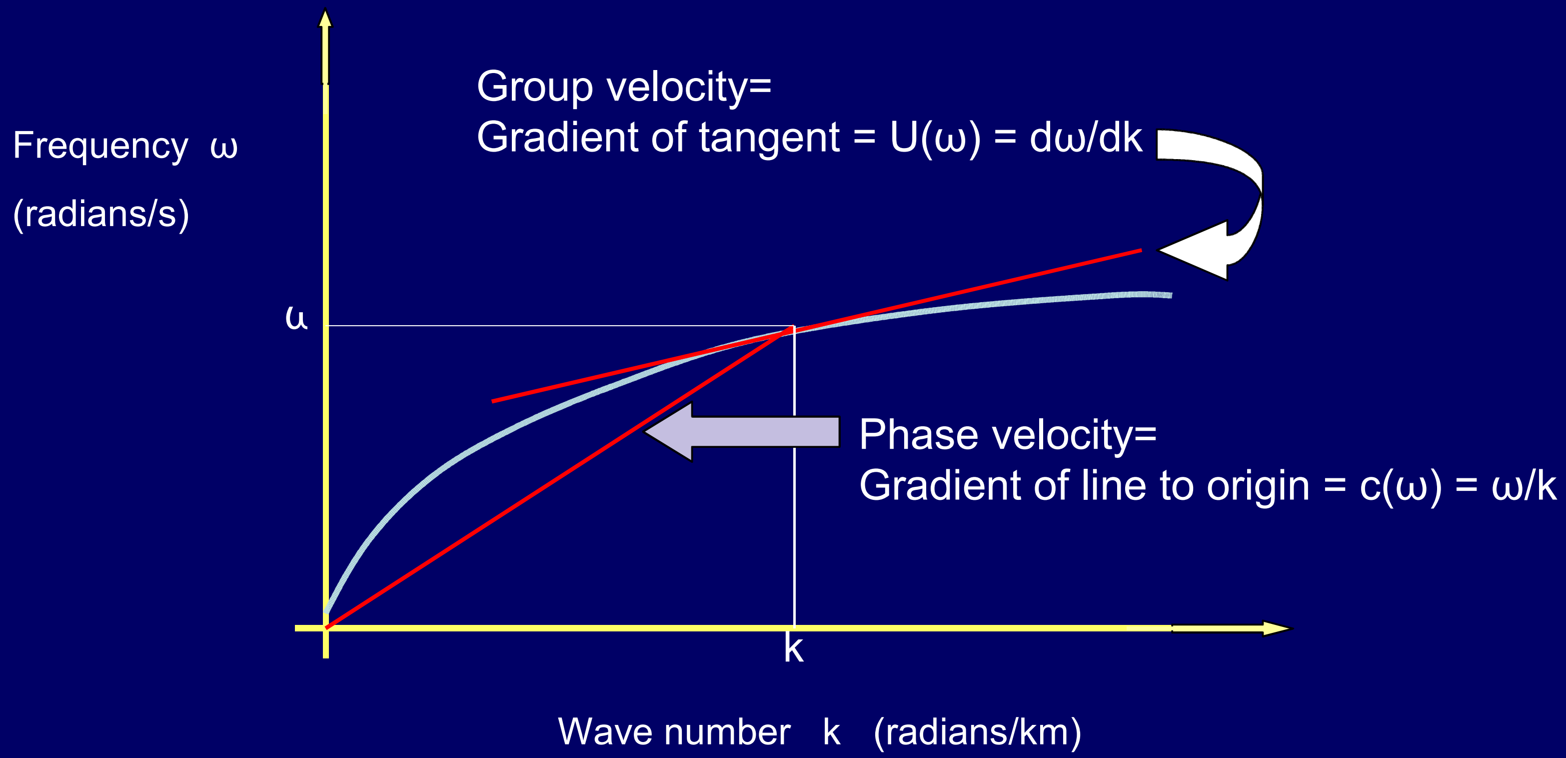

Examples of dispersed wave trains

Love waves: Kobe-Czech Republic

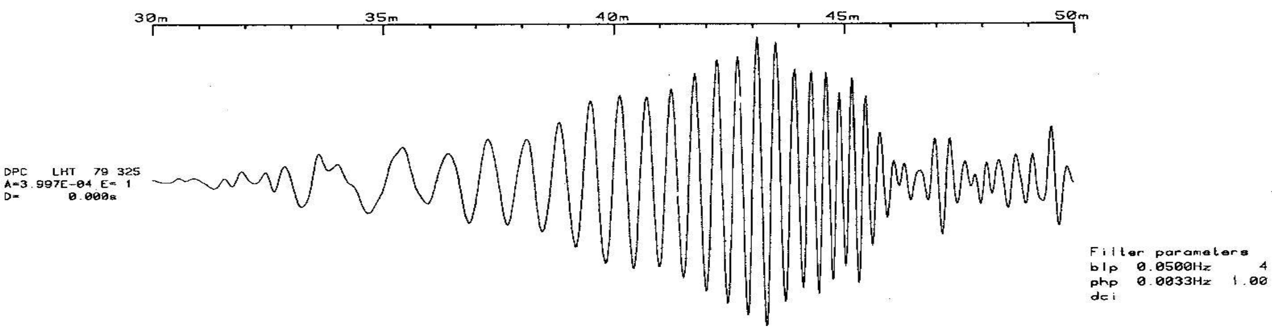

Rayleigh waves: Kobe-Afiamalu

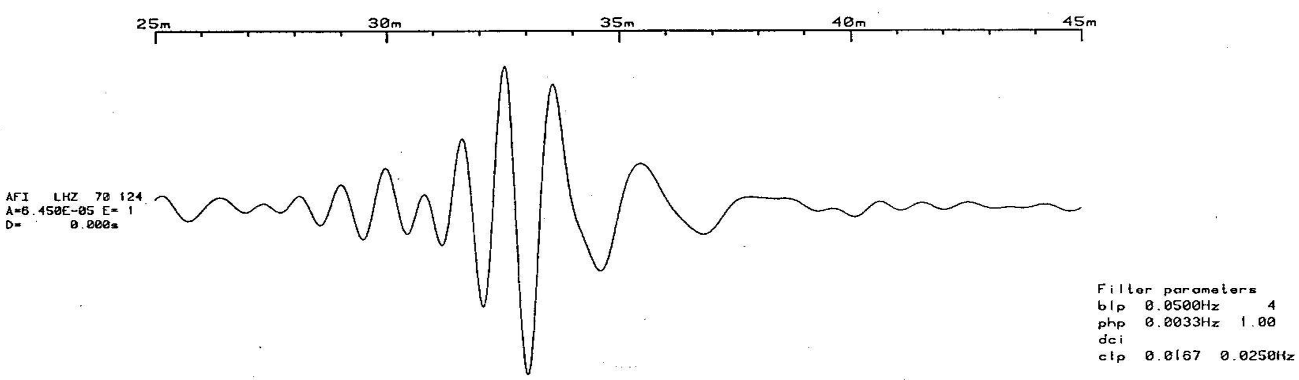

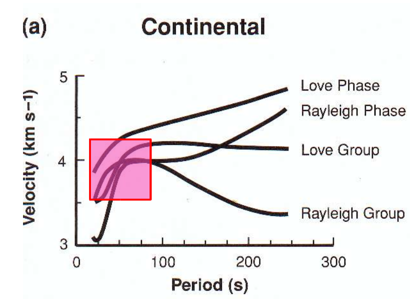

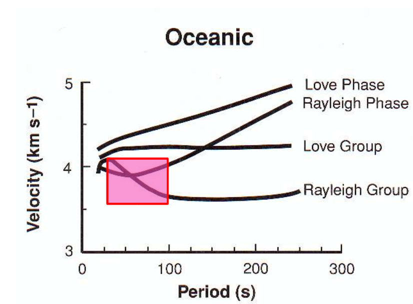

The principle of constructive interference and the analogy with the Somerfeld condition in atomic physics

THIRD BOHR POSTULATE

Number of wavelengths in the circumference = $a\,k$ = integer l

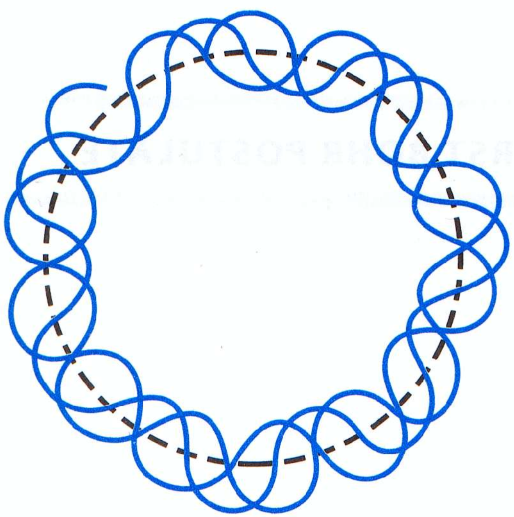

Figure 19.8 De Broglie electron waves around the circumference of a Bohr orbit in a case in which the electron wavelength does not satisfy the standing wave condition. The waves interfere to produce a net cancellation.

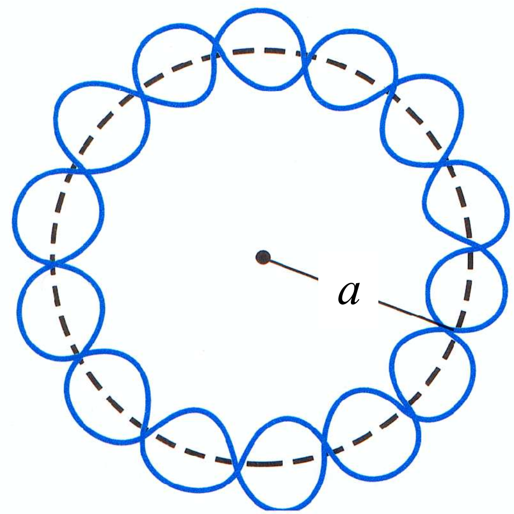

Figure 19.7 A standing de Broglie electron wave around th circumference of a Bohr orbit.

Thus normal modes can be thought of as the *standing* wave patterns set up by disturbances corresponding to propagating surface waves and overtones, and much can be learned about them by relating the properties of the standing wave patterns to the dispersion characteristics of travelling waves

Data (upper of each pair) and synthetics (lower of each pair) for three models. Δ = 99.5°. Mid-Atlantic ridge event recorded in W. Australia.

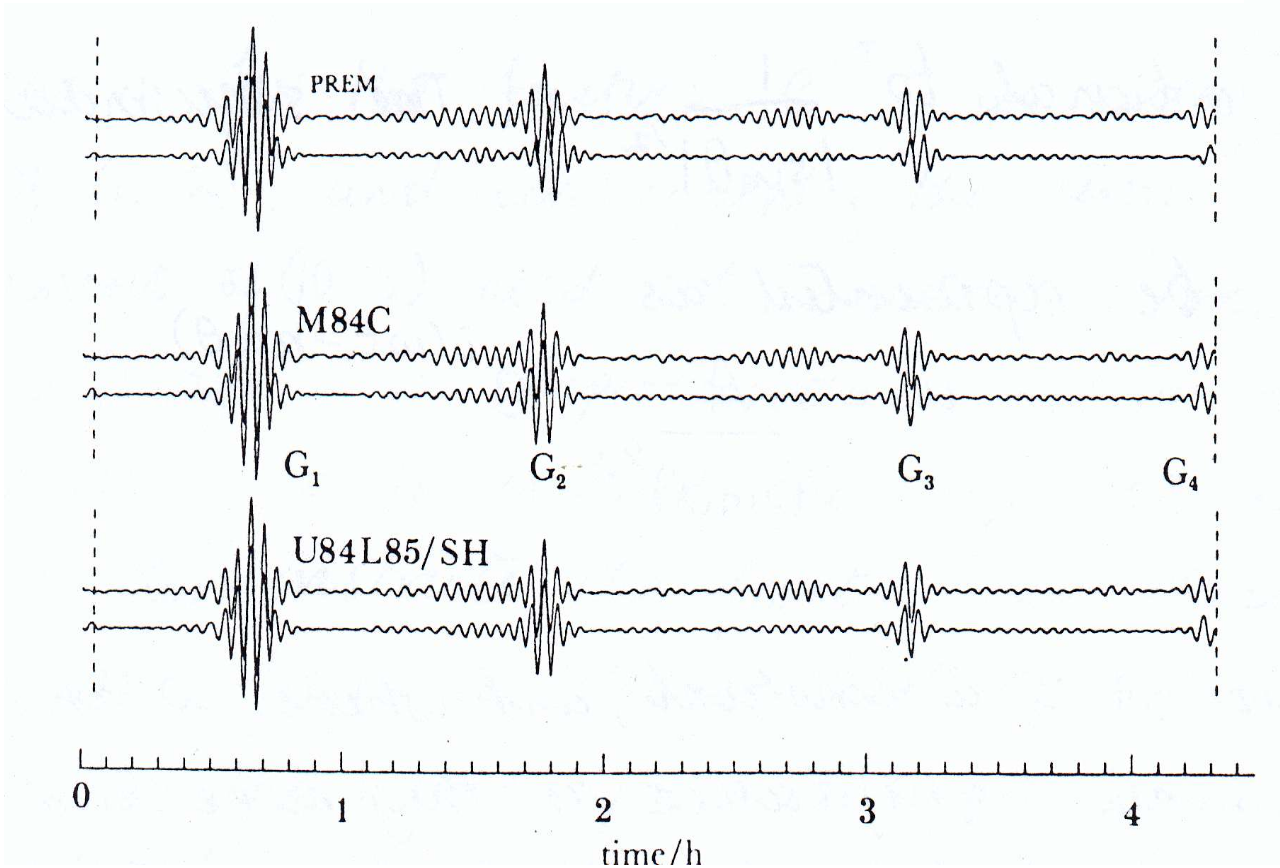

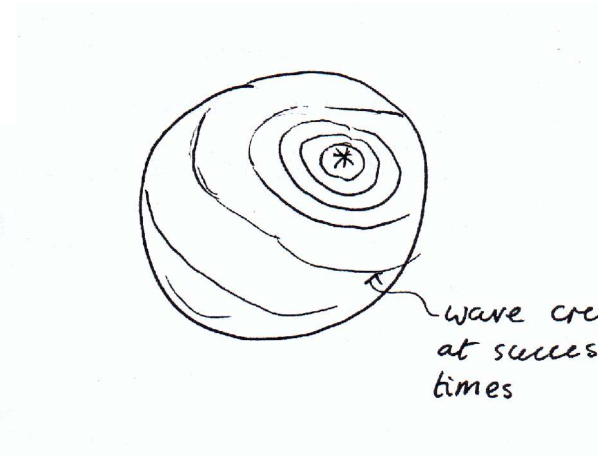

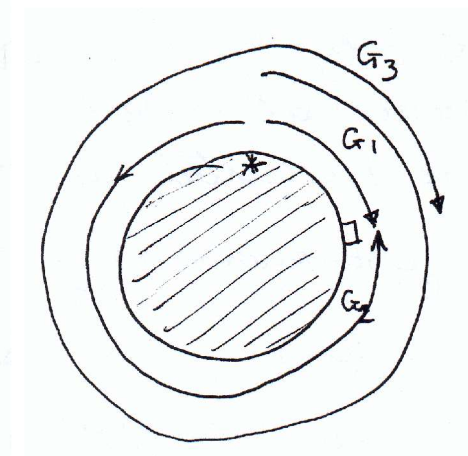

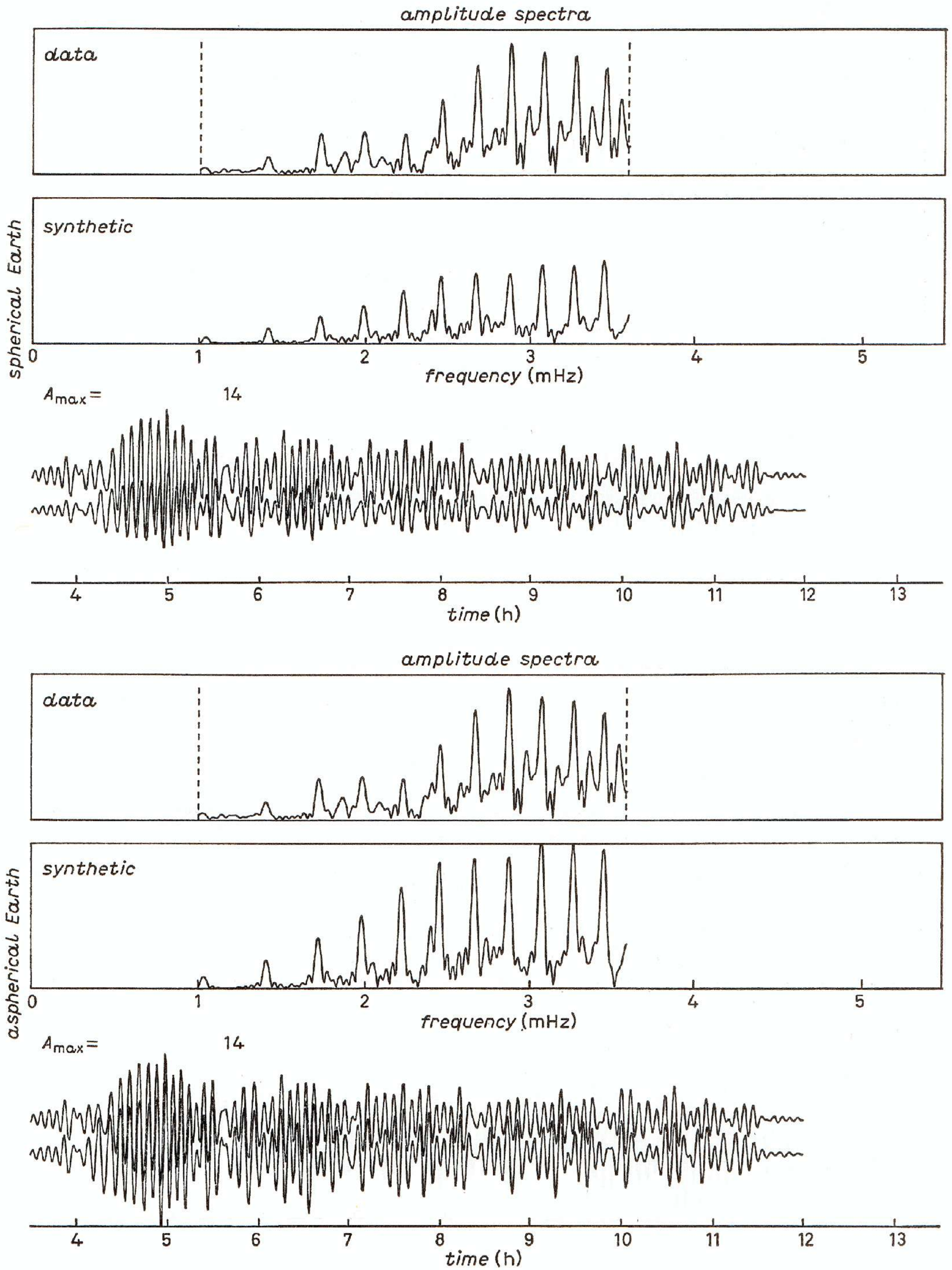
amplitude spectra
data
synthetic
spherical Earth
0
1
2
3
4
5
frequency (mHz)
A_{max} = 14
4
5
6
7
8
9
10
11
12
13
time (h)
amplitude spectra
data
synthetic
aspherical Earth
0
1
2
3
4
5
frequency (mHz)
A_{max} = 14
4
5
6
7
8
9
10
11
12
13
time (h)

Equations of Motion

Equations of motion link the seismic displacement field $\mathbf{u}(\mathbf{x}, t)$ and the pertubation in gravitational potential $\phi_1(\mathbf{x}, t)$.

The source, or excitation term can be represented in terms of an applied force distribution $F(\mathbf{x}, t)$. Symbolically, the equations of motion can then be written

$$(\mathbf{H} + \rho\,\partial_t^2)\,\mathbf{u} \;=\; \mathbf{F}$$

$\mathbf{H}$ is a complicated integro-differential operator in the spatial domain, incorporating the elastodynamic equations and the equations of gravitation.

$\mathbf{F} = \mathbf{F}(\mathbf{x}, t)$ is the *equivalent body force* distribution of the seismic source.

Taking the Fourier transform in time, we obtain

$$\mathbf{H}\bar{\mathbf{u}} + \rho\omega^2\bar{\mathbf{u}} \;=\; \bar{\mathbf{F}}$$

where $\bar{\mathbf{u}} = \bar{\mathbf{u}}(\mathbf{x}, \omega)$ is the temporal fourier transform of $\mathbf{u}(\mathbf{x}, t)$ etc.

$$(\mathbf{H} + \rho\omega^2)\bar{\mathbf{u}} \;=\; \bar{\mathbf{F}}$$

Thus we need to invert the operator on the left side, in order to solve for the displacement field $\mathbf{u}$ corresponding to a given force distribution $\mathbf{F}$. One method to do this is first to seek the eigenvalues and eigenfunctions of $\mathbf{H}$, and thus we are led to the eigenvalue problem

$$(\mathbf{H} + \rho\omega_k^2)\mathbf{s}_k \;=\; 0$$

where $\mathbf{s}_k = \mathbf{s}_k(\mathbf{x})$ is the "k-th" eigenfunction, and ω_k^2 is the corresponding eigenvalue.

Then representing the displacement field $\mathbf{u}(\mathbf{x}, t)$ as a sum over eigenfunctions:

$$\mathbf{u}(\mathbf{x}, t) \;=\; \sum_k a_k(t)\mathbf{s}_k(\mathbf{x})$$

We can solve for the excitation amplitudes $a_k(t)$. We find

$$a_k(t) \;=\; \frac{1}{\omega_k^2}\int_{-\infty}^{t} [1 - \cos\omega_k(t - t')]\dot{F}_k(t')\mathrm{d}t'$$

where

$$F_k(t) \;=\; \frac{\int_V \bar{s}_k \cdot \mathbf{F}(\mathbf{x}, t)\mathrm{dv}}{\int_V \rho\bar{s}_k(\mathbf{x}) \cdot \mathbf{s}_k(\mathbf{x})\mathrm{dv}}$$

Eigenfunctions and Eigenvalues

Defining vector spherical harmonics

$$
\begin{aligned}
\mathbf{P}_l^m &= \hat{\mathbf{r}}\, Y_l^m(\theta,\phi) \\
\mathbf{B}_l^m &= \nabla_1\, Y_l^m(\theta,\phi) \\
\mathbf{C}_l^m &= -\hat{\mathbf{r}} \times \nabla_1\, Y_l^m(\theta,\phi)
\end{aligned}
$$

where $\nabla_1 = \widehat{\boldsymbol{\theta}}\,\partial_\theta + \operatorname{cosec}\theta\,\widehat{\boldsymbol{\phi}}\,\partial_\phi$, we write

$$
\mathbf{s}_k(\mathbf{x}) = U(r)\mathbf{P}_l^m + V(r)\mathbf{B}_l^m + W(r)\mathbf{C}_l^m
$$

Where r is the radial coordinate. The it scalar eigenfunctions $U(r)$, $V(r)$, $W(r)$ satisfy a set of linear ordinary differential equations in r. These can be written in matrix form:

$$
\frac{d\mathbf{y}}{dr} = \mathbf{A}(r)\mathbf{y}
$$

subject to the appropriate boundary conditions at the centre of the earth, at internal discontinuities and at the free surface. Thus we obtain an eigenvalue problem for ω_k^2. This eigenvalue problem depends on the spherical harmonic order l but not on the degree m. i.e. the eigenvalues are degenerate in m yielding $2l+1$ $(-l \le m \le l)$ different eigenfunctions $\mathbf{s}_k$ belonging to the same eigenvalue ω_k^2.

The equations for $U(r)$, $V(r)$, and the corresponding perturbation to the gravitational potential represented by $P(r)$, together with their radial derivatives, constitute a 6th order system for *spheroidal* or it poloidal modes. These correspond to Rayleigh waves and P-SV body waves.

The equations for $W(r)$ and its derivative constitute a 2nd order system for *toridal* modes. These correspond to Love waves and SH body waves.

Indicative shapes of the spherical harmononics of low degree *l* and order *m*

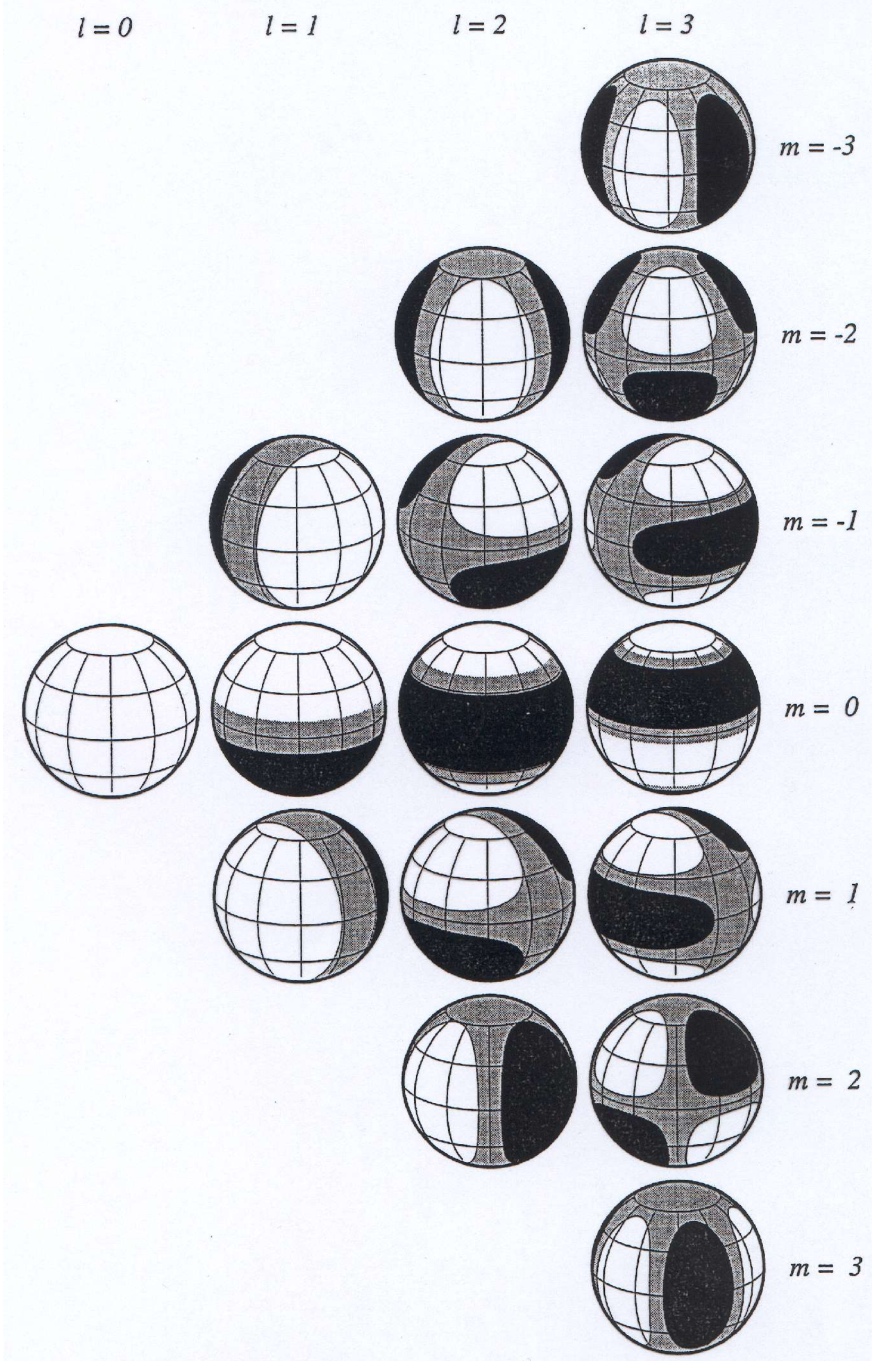

Surface shapes of spherical harmonics for higher *l* and *m*

l=10 m=0 ***l=20 m=10*** ***l=32 m=30*** ***l=30 m=30***

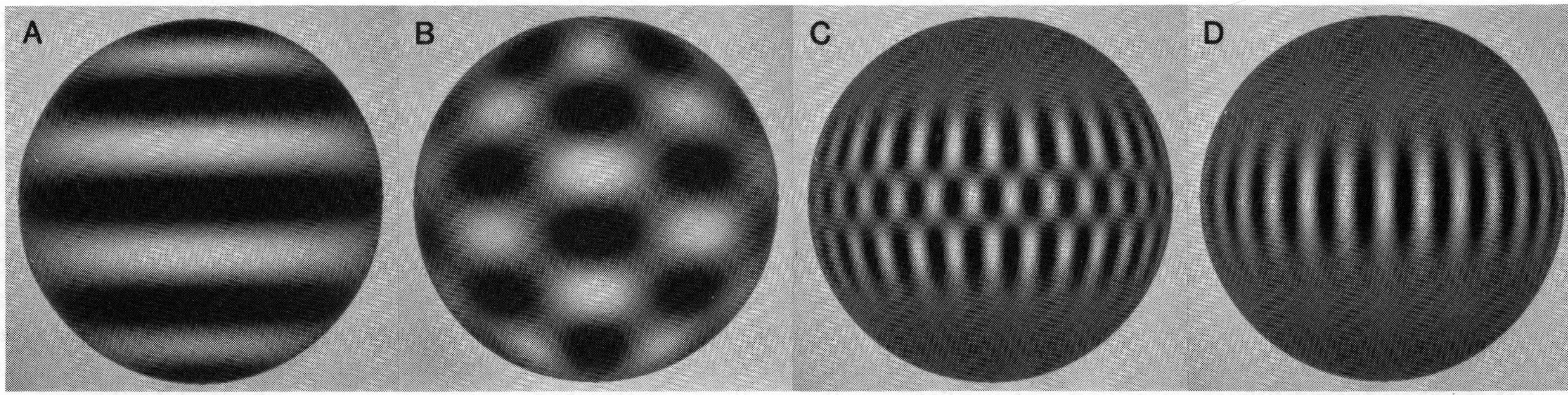

Fig. 3. Doppler velocities of solar p modes. The shading represents the line-of-sight component of velocity: dark regions are approaching the observer and light regions are receding (or vice versa). The motion is almost radial, so that the mid-grey at the edges of the sun's image represents zero velocity. (A) The zonal mode ($m = 0$) of degree $l = 10$; (B and C) tesseral modes with $(l, m) = (20, 10)$ and $(32, 30)$; (D) a sectoral mode ($m = l$) of degree 30.

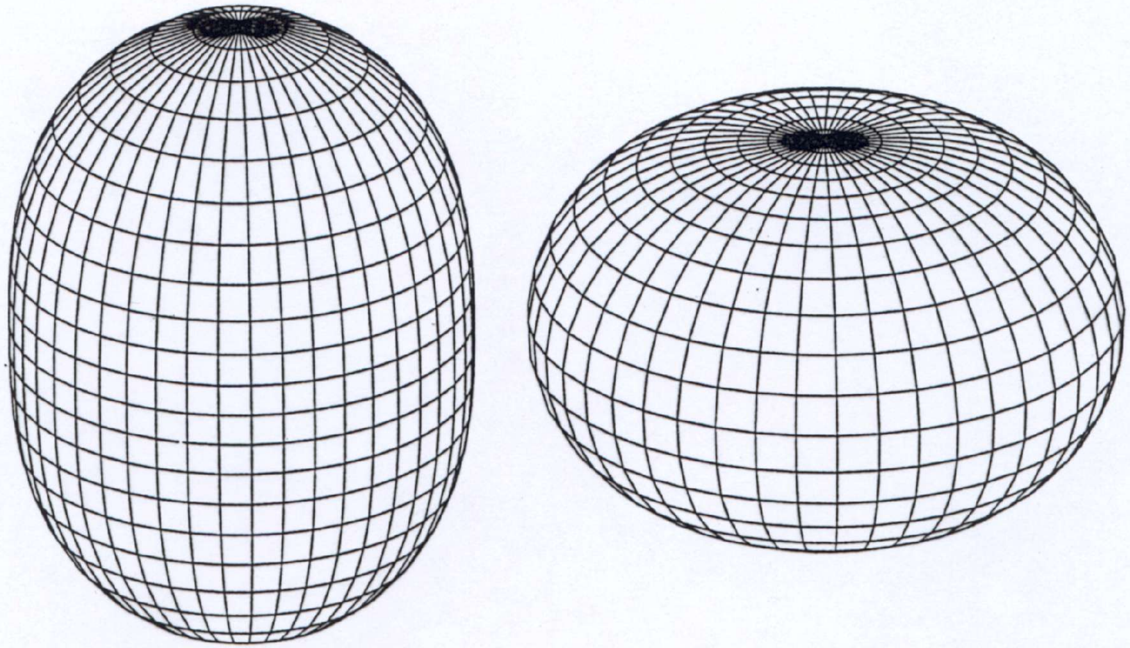

Fig. 8.12. A highly exaggerated picture of the normal mode ${}_0S_2$. This mode has a period of about 54 minutes; the two images are separated in time by 27 minutes.

Event 21 May 1998 (Indonesia) a TSUM (Tsumeb, Namibia)
(Depth = 28 km; Mw = 6.6; Mb = 6.3 Δ = 101.5°)

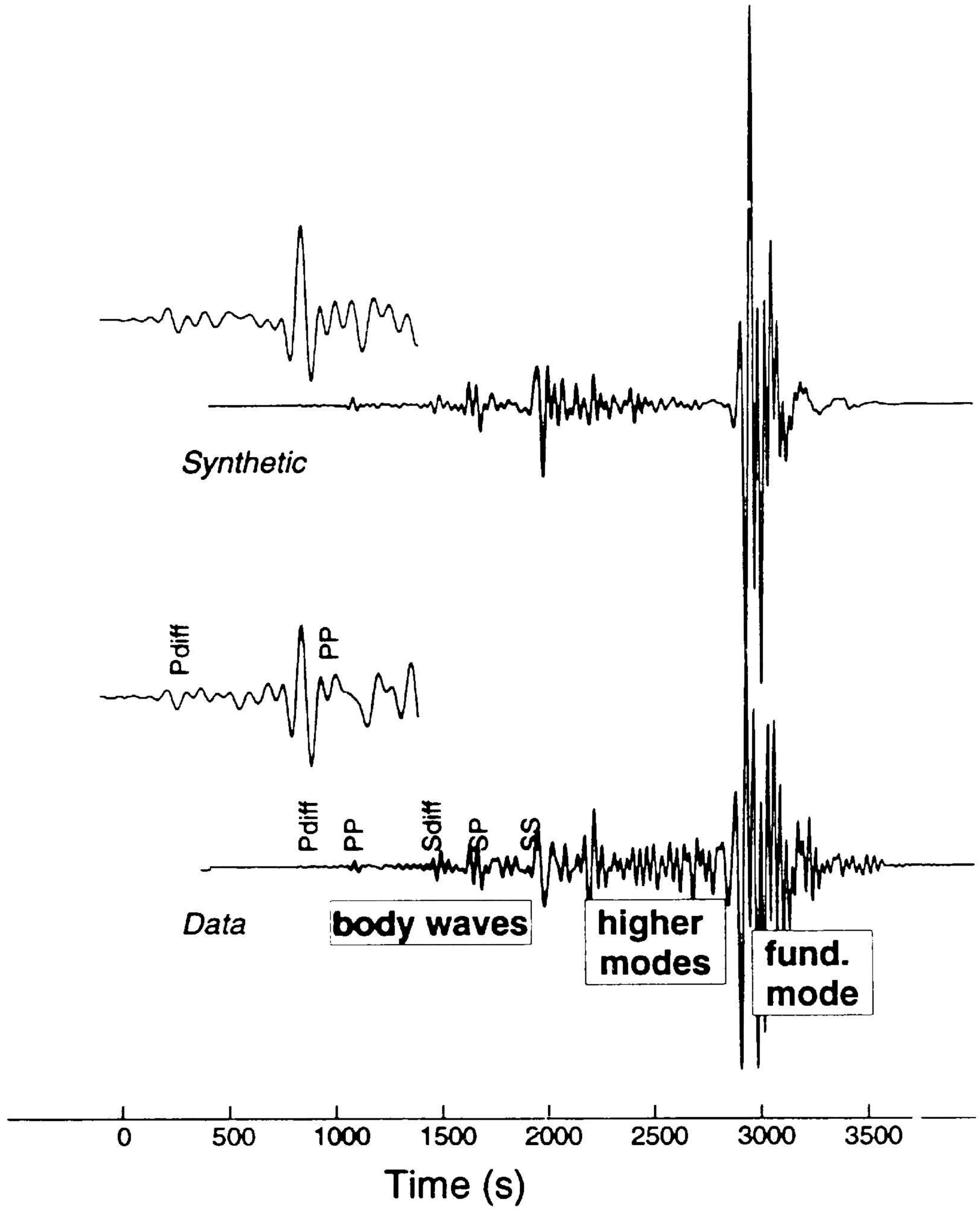

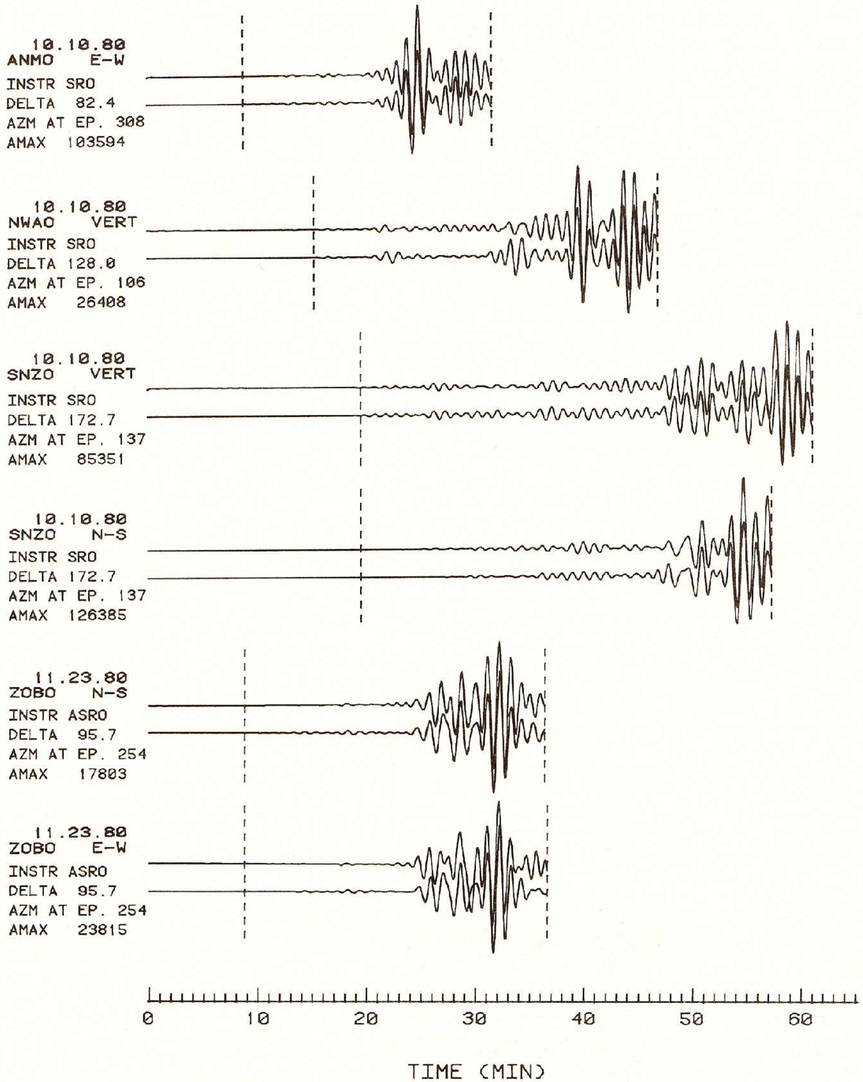

Fig. 3a — Examples of fitting (r.m.s. $\sim$ 0.3-0.4) between waveform data (top record) and synthetic seismogram (bottom record) for body-waves, low-pass filtered with a cut-off period of 45 s. For each trace the SRO/ASRO station and the type of instrument (vertical, North-South, East-West) are indicated. The maximum amplitude of the trace represents the ditigal SRO count. Angular distance and azimuth of the station are also indicated. Only data included between the dashed vertical lines are used in the inversion. The examples shown are records of the Irpinia event (Nov. 23, 1980) and of the main shock in El Asnam (Algeria, Oct. 10, 1980). The time scale reports the time elapsed from the origin time.

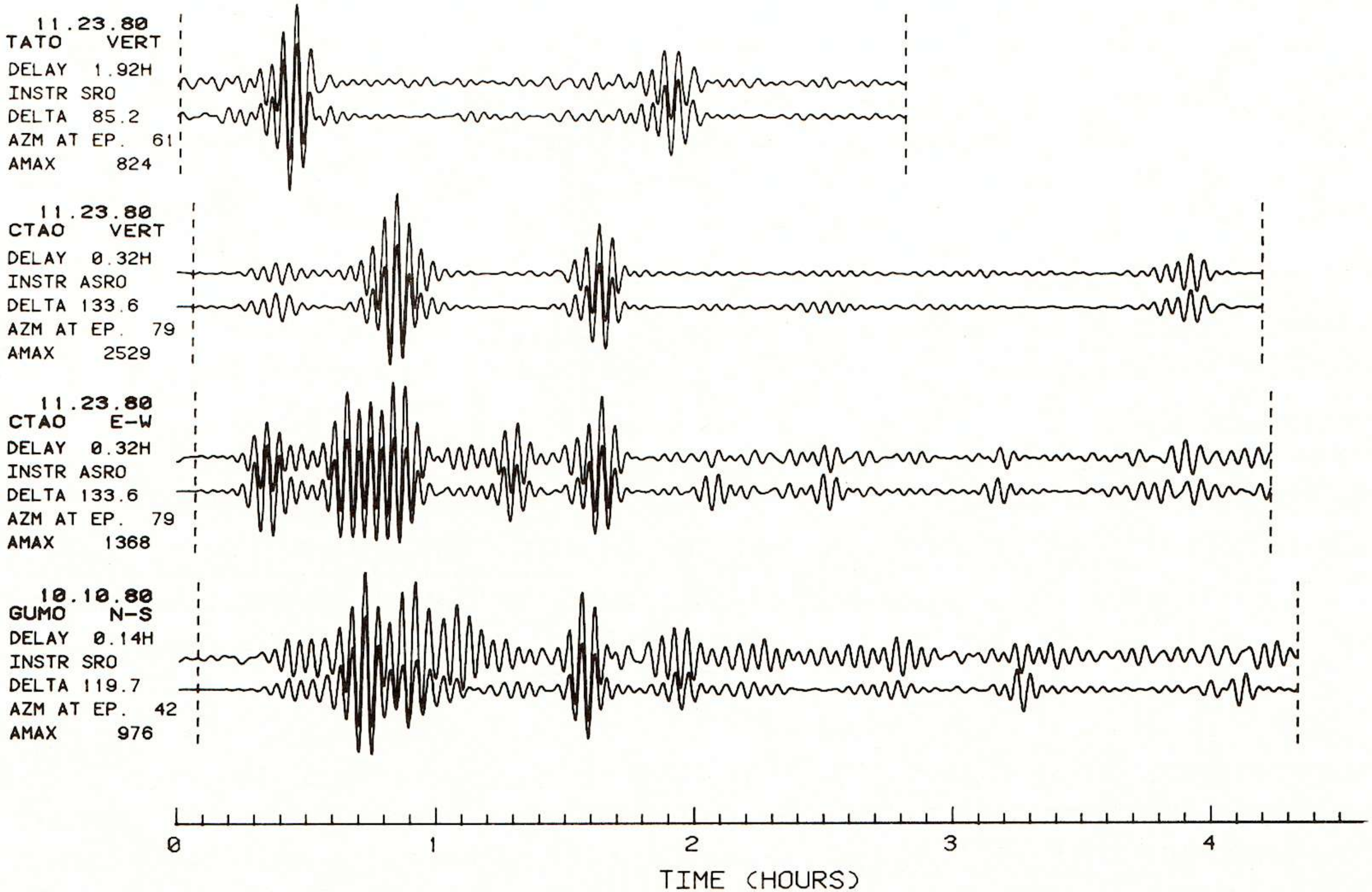

Fig. 3c — Comparison of waveform data and synthetic seismograms for mantle waves generated by the same events shown in Fig. 3a. A low-pass filter with a cut-off period of 135 s is used. The delay time represents the time elapsed from the origin time to the beginning of the record used in the inversion.

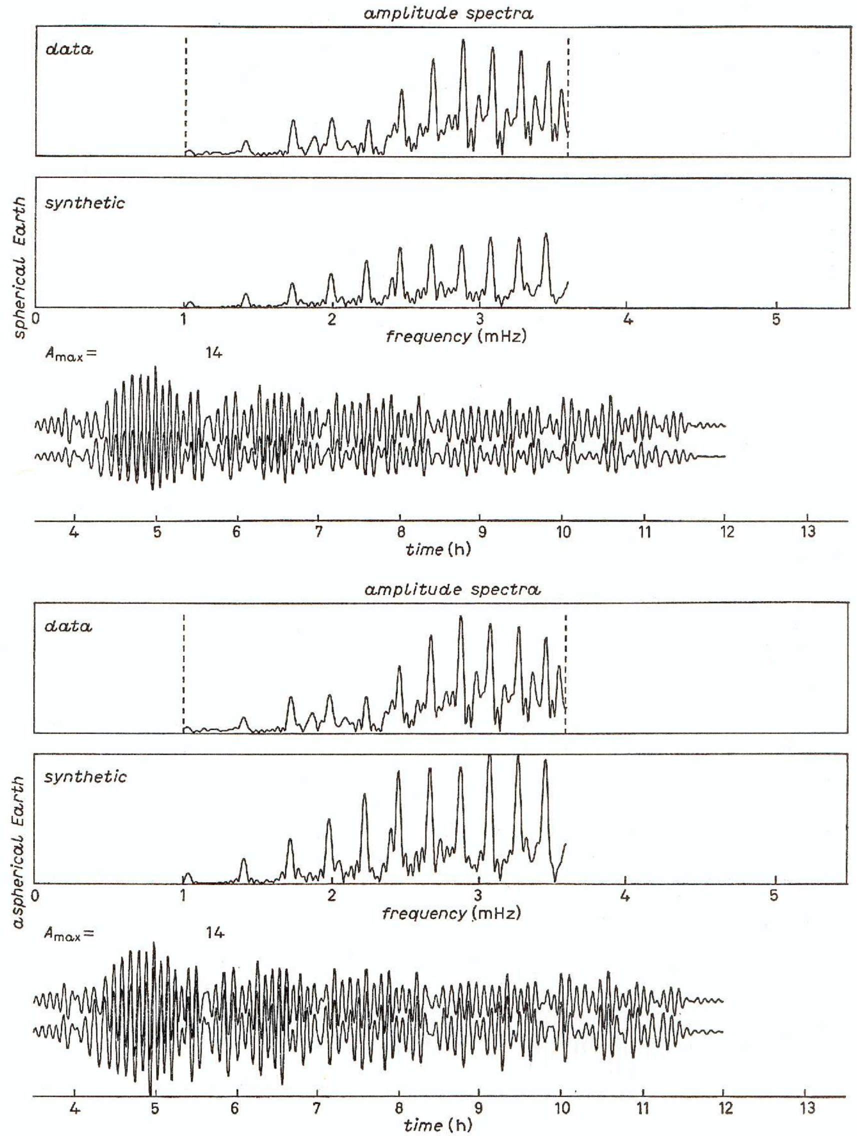

Fig. 3*a*. – Comparison of data and synthetic seismograms for the « Eureka » earthquake off the coast of N. California, date 8/11/1980, origin time 10.27.34.0, published hypocentral co-ordinates: latitude 41.12 °N, longitude 124.25 °W, depth 19.00 km. IDA station BDF, starting time of the record relative to the origin time 12626.5 s, angular distance 90.23°, azimuth of receiver from source 110.59°, azimuth of source from receiver 312.76°. The aspherical model is that shown in fig. 2.

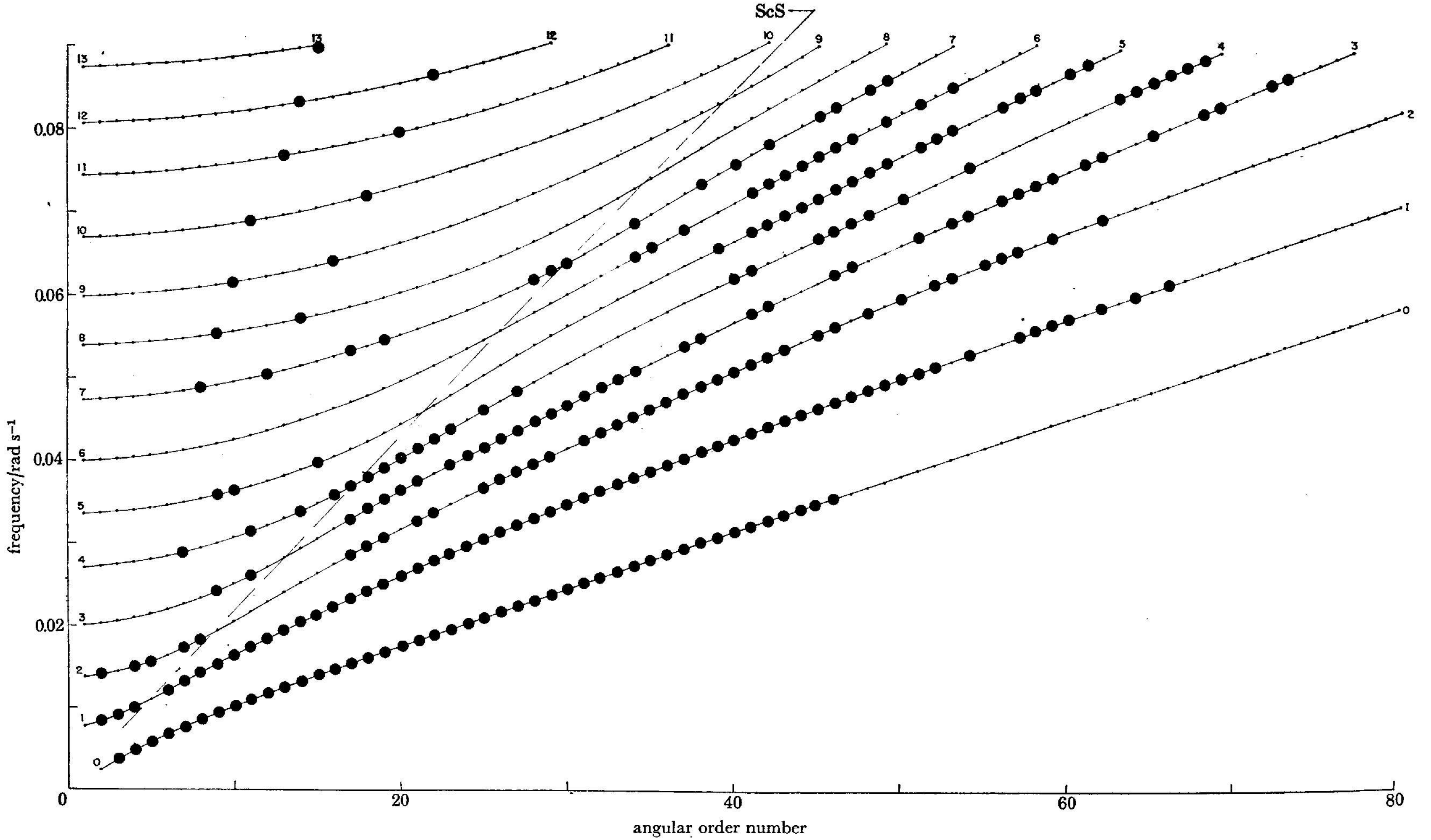

Figure 2.1a Toroidal normal modes in the (ω, l) plane. The large dots indicate observed modes used in the inversions of Gilbert and Dziewonski (1975), from whose paper the figure is taken.

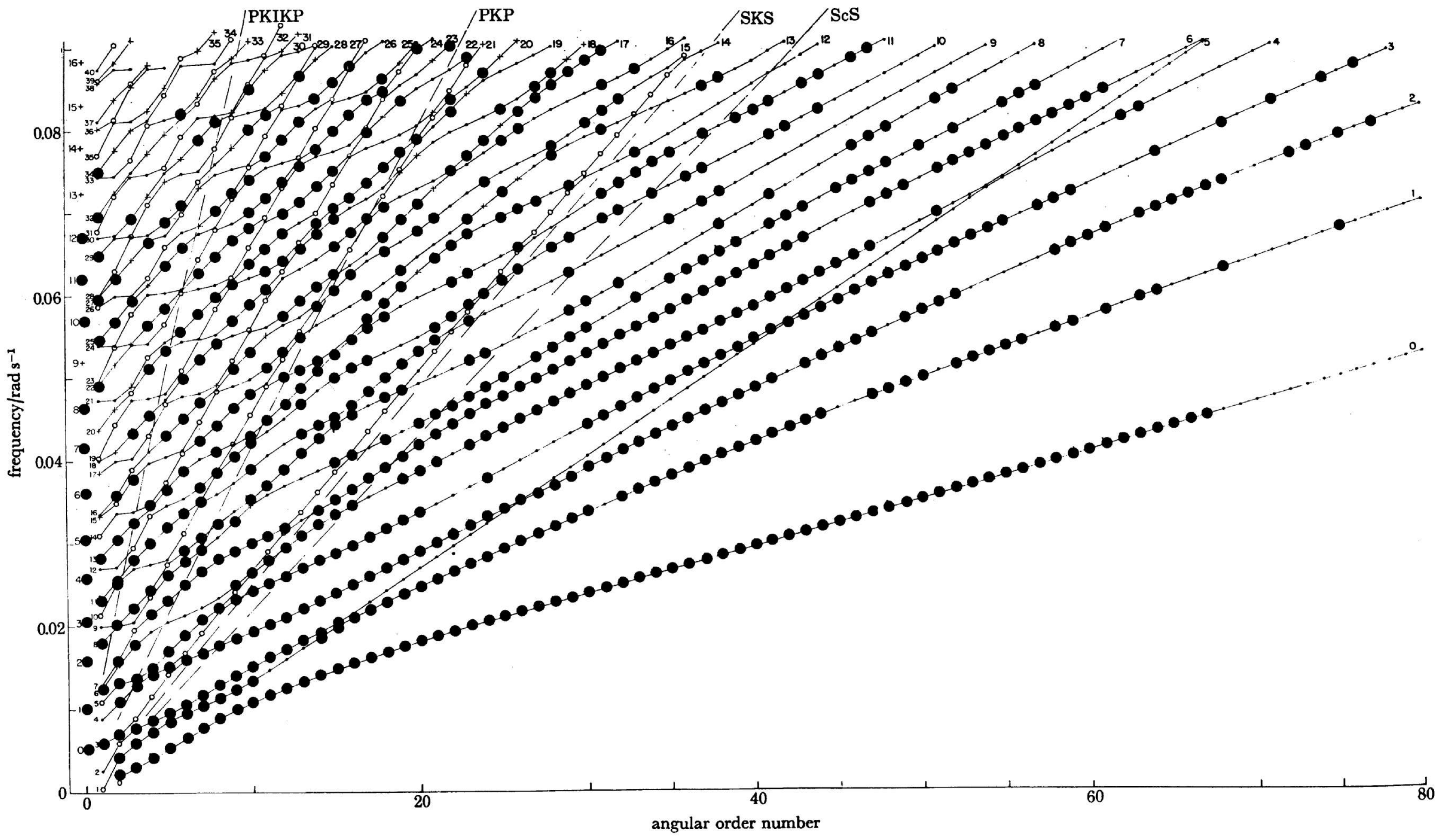

Figure 2.1b Spheroidal normal modes in the (ω, l) plane (from Gilbert and Dziewonski, 1975).

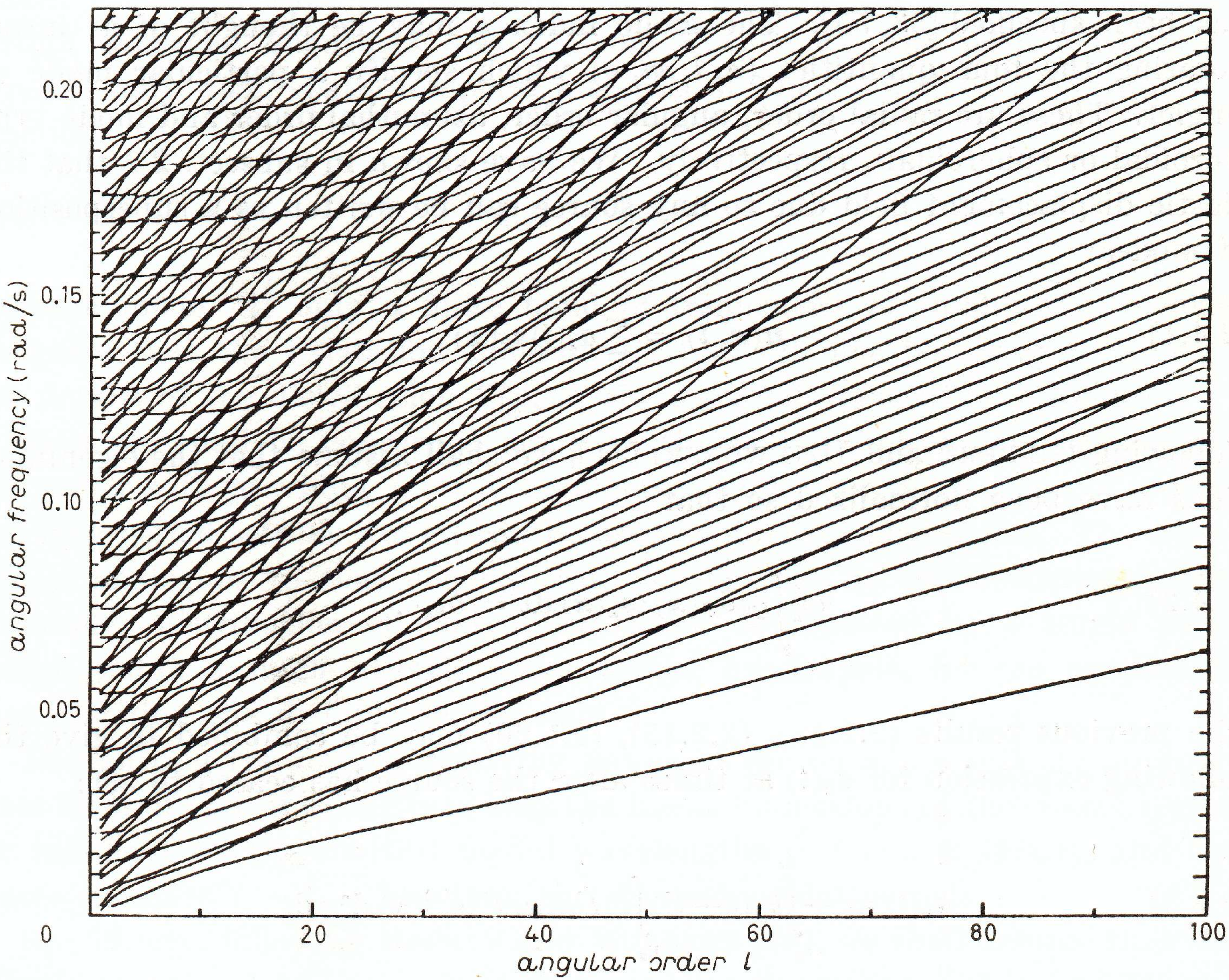

Fig. 2.1. – A dispersion diagram for the PREM model for frequencies up to 35 mHz. The diagram represents the eigenfrequencies of spheroidal free oscillations as functions of angular order. The lowest curve is the fundamental-mode branch.

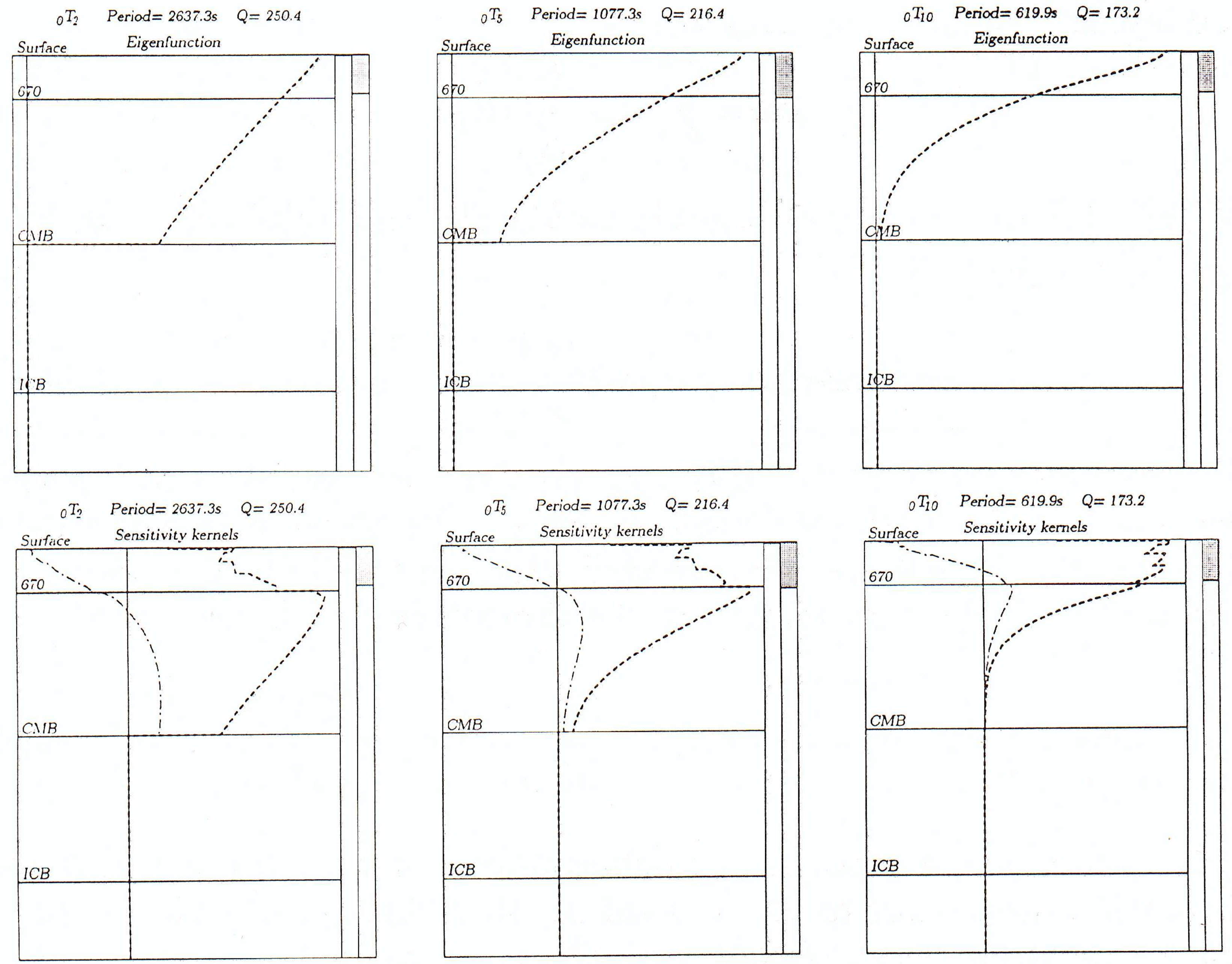

$_0T_2$ Period= 2637.3s Q= 250.4
Eigenfunction
Surface
670
CMB
ICB
$_0T_5$ Period= 1077.3s Q= 216.4
Eigenfunction
Surface
670
CMB
ICB
$_0T_{10}$ Period= 619.9s Q= 173.2
Eigenfunction
Surface
670
CMB
ICB
$_0T_2$ Period= 2637.3s Q= 250.4
Sensitivity kernels
Surface
670
CMB
ICB
$_0T_5$ Period= 1077.3s Q= 216.4
Sensitivity kernels
Surface
670
CMB
ICB
$_0T_{10}$ Period= 619.9s Q= 173.2
Sensitivity kernels
Surface
670
CMB
ICB

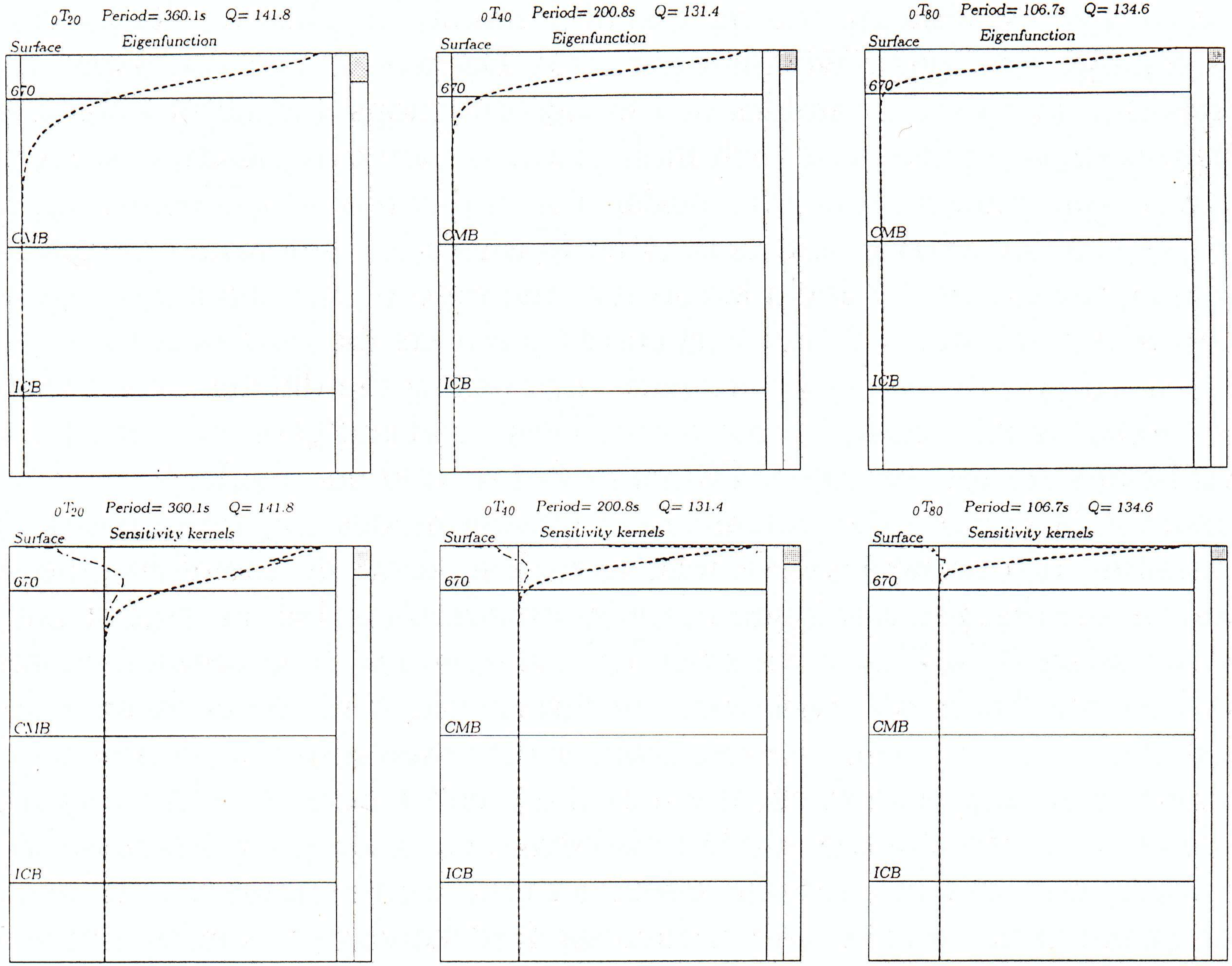

$_0T_{20}$ Period= 360.1s Q= 141.8
Eigenfunction
Surface
670
CMB
ICB
$_0T_{40}$ Period= 200.8s Q= 131.4
Eigenfunction
Surface
670
CMB
ICB
$_0T_{80}$ Period= 106.7s Q= 134.6
Eigenfunction
Surface
670
CMB
ICB
$_0T_{20}$ Period= 360.1s Q= 141.8
Sensitivity kernels
Surface
670
CMB
ICB
$_0T_{40}$ Period= 200.8s Q= 131.4
Sensitivity kernels
Surface
670
CMB
ICB
$_0T_{80}$ Period= 106.7s Q= 134.6
Sensitivity kernels
Surface
670
CMB
ICB

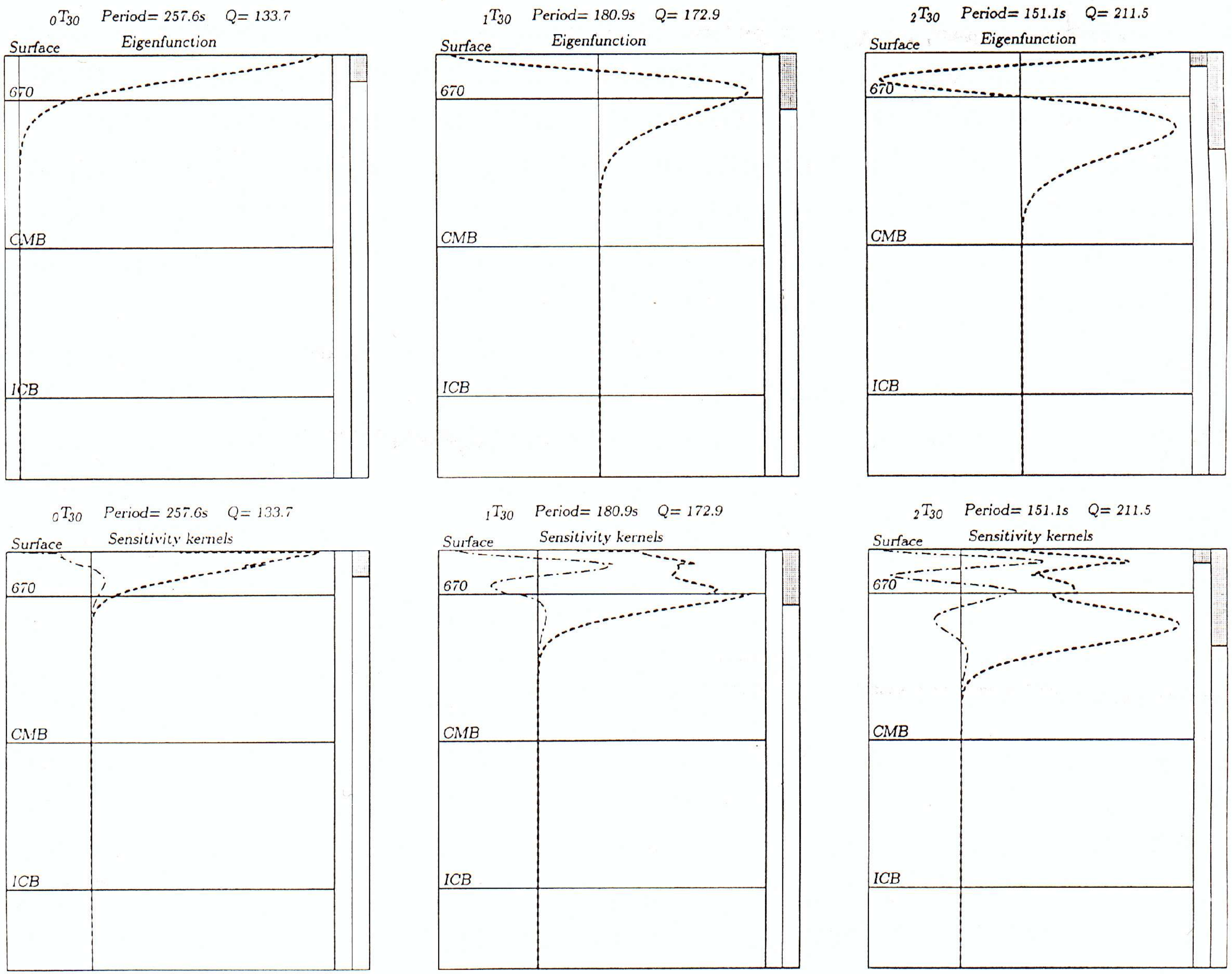

$_0T_{30}$ Period= 257.6s Q= 133.7
Eigenfunction
Surface
670
CMB
ICB
$_1T_{30}$ Period= 180.9s Q= 172.9
Eigenfunction
Surface
670
CMB
ICB
$_2T_{30}$ Period= 151.1s Q= 211.5
Eigenfunction
Surface
670
CMB
ICB
$_0T_{30}$ Period= 257.6s Q= 133.7
Sensitivity kernels
Surface
670
CMB
ICB
$_1T_{30}$ Period= 180.9s Q= 172.9
Sensitivity kernels
Surface
670
CMB
ICB
$_2T_{30}$ Period= 151.1s Q= 211.5
Sensitivity kernels
Surface
670
CMB
ICB

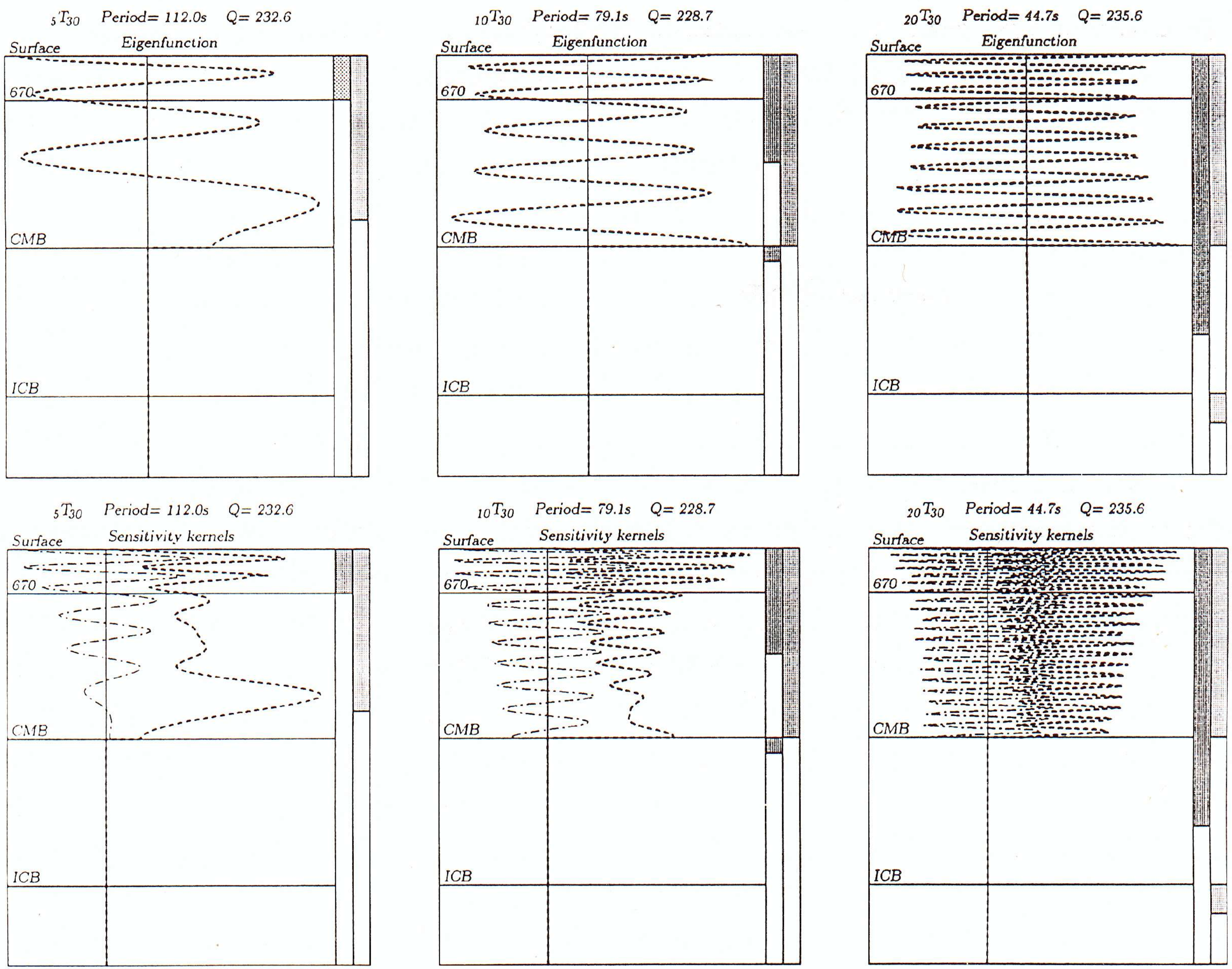

$_5T_{30}$ Period= 112.0s Q= 232.6
Eigenfunction
$_{10}T_{30}$ Period= 79.1s Q= 228.7
Eigenfunction
$_{20}T_{30}$ Period= 44.7s Q= 235.6
Eigenfunction
Surface
670
CMB
ICB
$_5T_{30}$ Period= 112.0s Q= 232.6
Sensitivity kernels
$_{10}T_{30}$ Period= 79.1s Q= 228.7
Sensitivity kernels
$_{20}T_{30}$ Period= 44.7s Q= 235.6
Sensitivity kernels

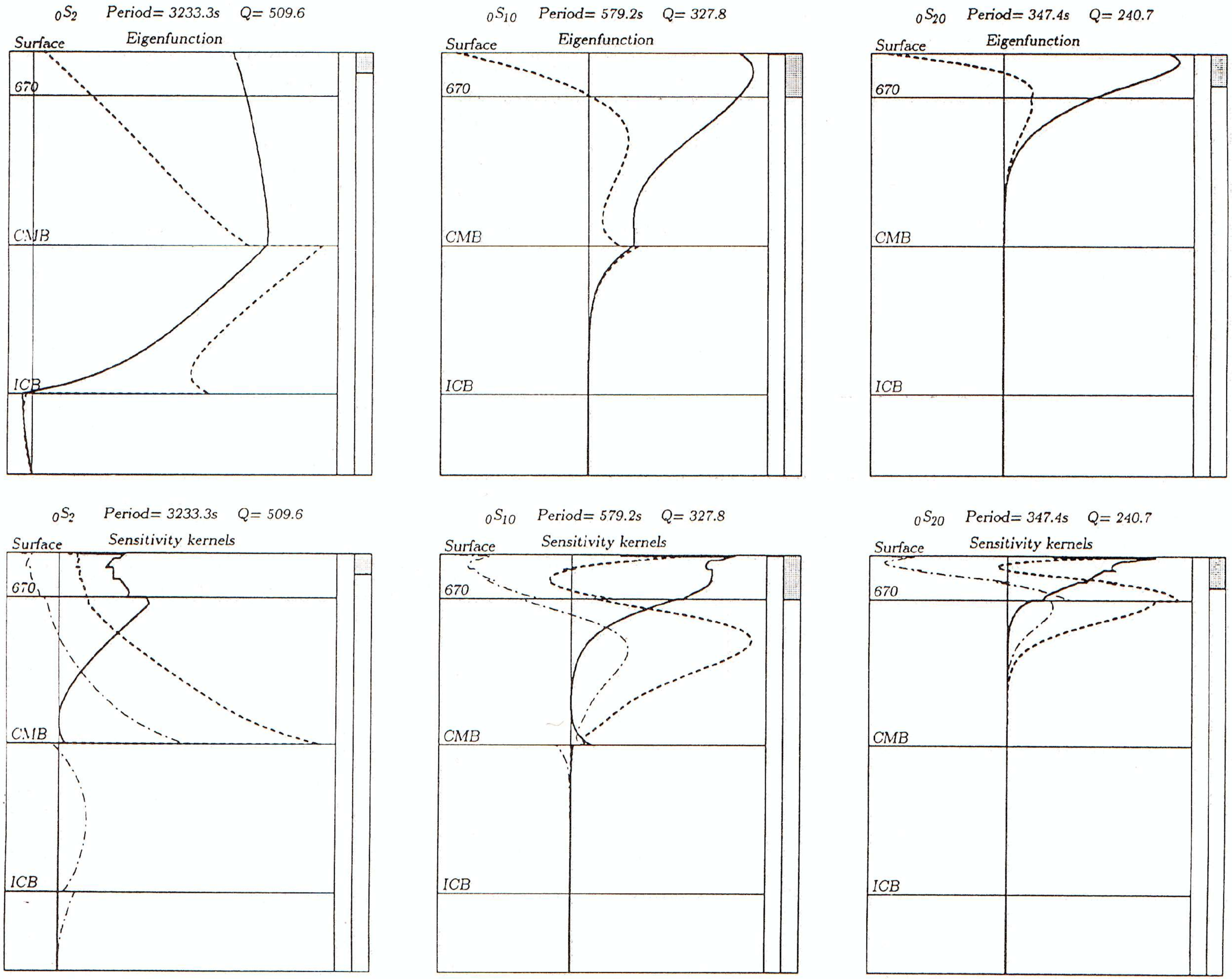

$_0S_2$ Period= 3233.3s Q= 509.6
Surface
Eigenfunction
670
CMB
ICB
$_0S_{10}$ Period= 579.2s Q= 327.8
Surface
Eigenfunction
670
CMB
ICB
$_0S_{20}$ Period= 347.4s Q= 240.7
Surface
Eigenfunction
670
CMB
ICB
$_0S_2$ Period= 3233.3s Q= 509.6
Surface
Sensitivity kernels
670
CMB
ICB
$_0S_{10}$ Period= 579.2s Q= 327.8
Surface
Sensitivity kernels
670
CMB
ICB
$_0S_{20}$ Period= 347.4s Q= 240.7
Surface
Sensitivity kernels
670
CMB
ICB

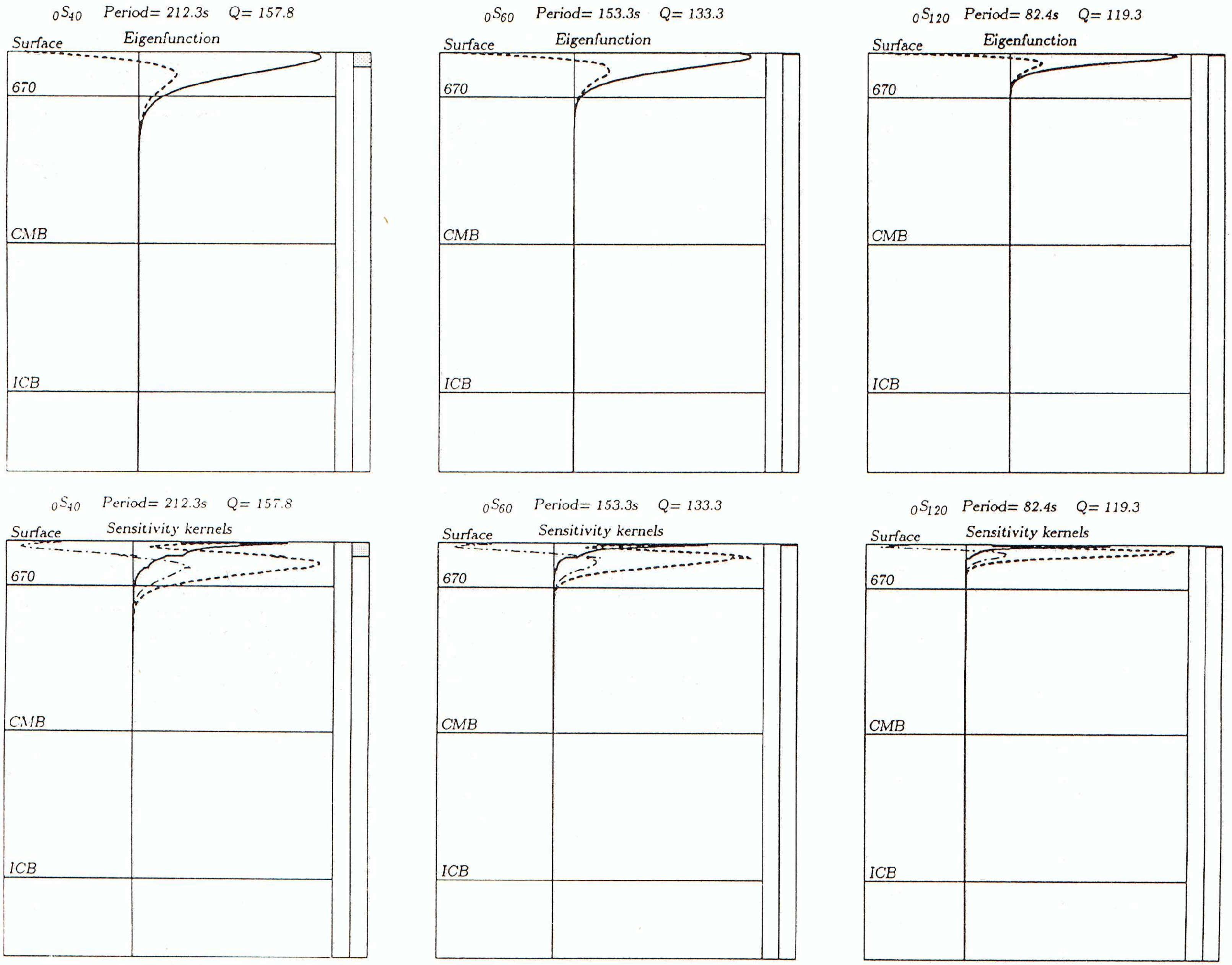

$_0S_{40}$ Period= 212.3s Q= 157.8
Eigenfunction
Surface
670
CMB
ICB
$_0S_{60}$ Period= 153.3s Q= 133.3
Eigenfunction
Surface
670
CMB
ICB
$_0S_{120}$ Period= 82.4s Q= 119.3
Eigenfunction
Surface
670
CMB
ICB
$_0S_{40}$ Period= 212.3s Q= 157.8
Sensitivity kernels
Surface
670
CMB
ICB
$_0S_{60}$ Period= 153.3s Q= 133.3
Sensitivity kernels
Surface
670
CMB
ICB
$_0S_{120}$ Period= 82.4s Q= 119.3
Sensitivity kernels
Surface
670
CMB
ICB

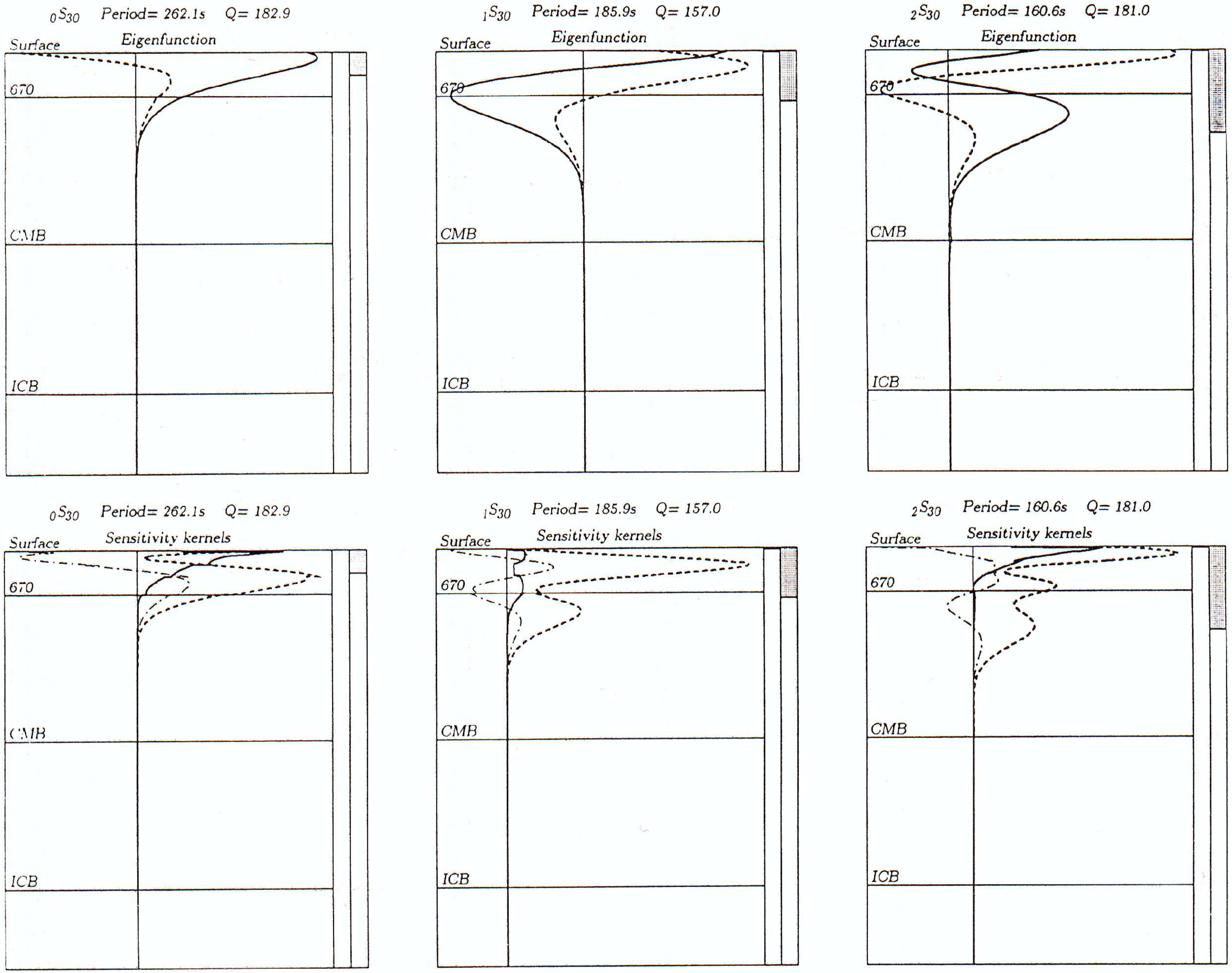

$_0S_{30}$ Period= 262.1s Q= 182.9
Eigenfunction
Surface
670
CMB
ICB
$_1S_{30}$ Period= 185.9s Q= 157.0
Eigenfunction
Surface
670
CMB
ICB
$_2S_{30}$ Period= 160.6s Q= 181.0
Eigenfunction
Surface
670
CMB
ICB
$_0S_{30}$ Period= 262.1s Q= 182.9
Sensitivity kernels
Surface
670
CMB
ICB
$_1S_{30}$ Period= 185.9s Q= 157.0
Sensitivity kernels
Surface
670
CMB
ICB
$_2S_{30}$ Period= 160.6s Q= 181.0
Sensitivity kernels
Surface
670
CMB
ICB

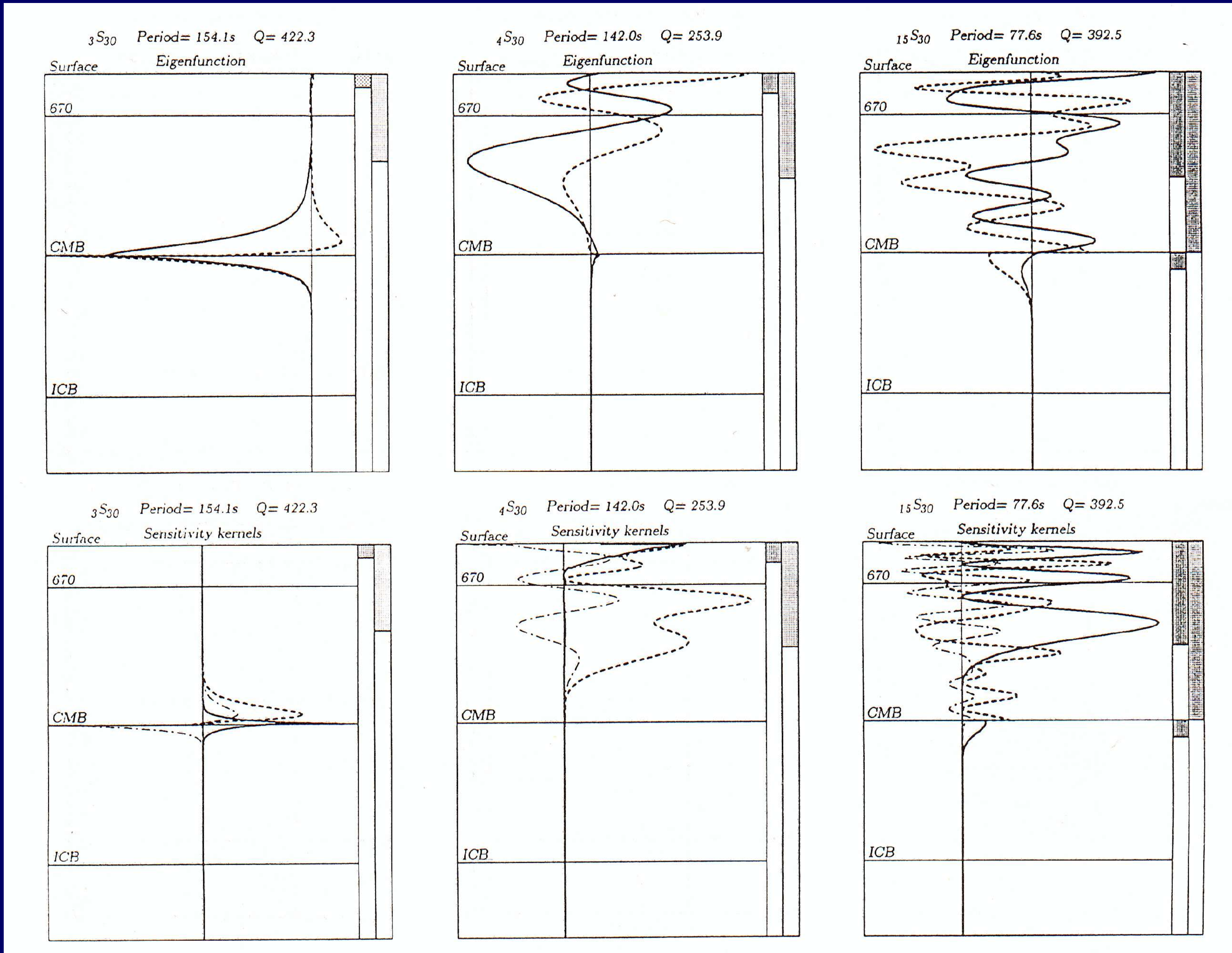
$_3S_{30}$ Period= 154.1s Q= 422.3
Eigenfunction
Surface
670
CMB
ICB
$_4S_{30}$ Period= 142.0s Q= 253.9
Eigenfunction
Surface
670
CMB
ICB
$_{15}S_{30}$ Period= 77.6s Q= 392.5
Eigenfunction
Surface
670
CMB
ICB
$_3S_{30}$ Period= 154.1s Q= 422.3
Sensitivity kernels
Surface
670
CMB
ICB
$_4S_{30}$ Period= 142.0s Q= 253.9
Sensitivity kernels
Surface
670
CMB
ICB
$_{15}S_{30}$ Period= 77.6s Q= 392.5
Sensitivity kernels
Surface
670
CMB
ICB

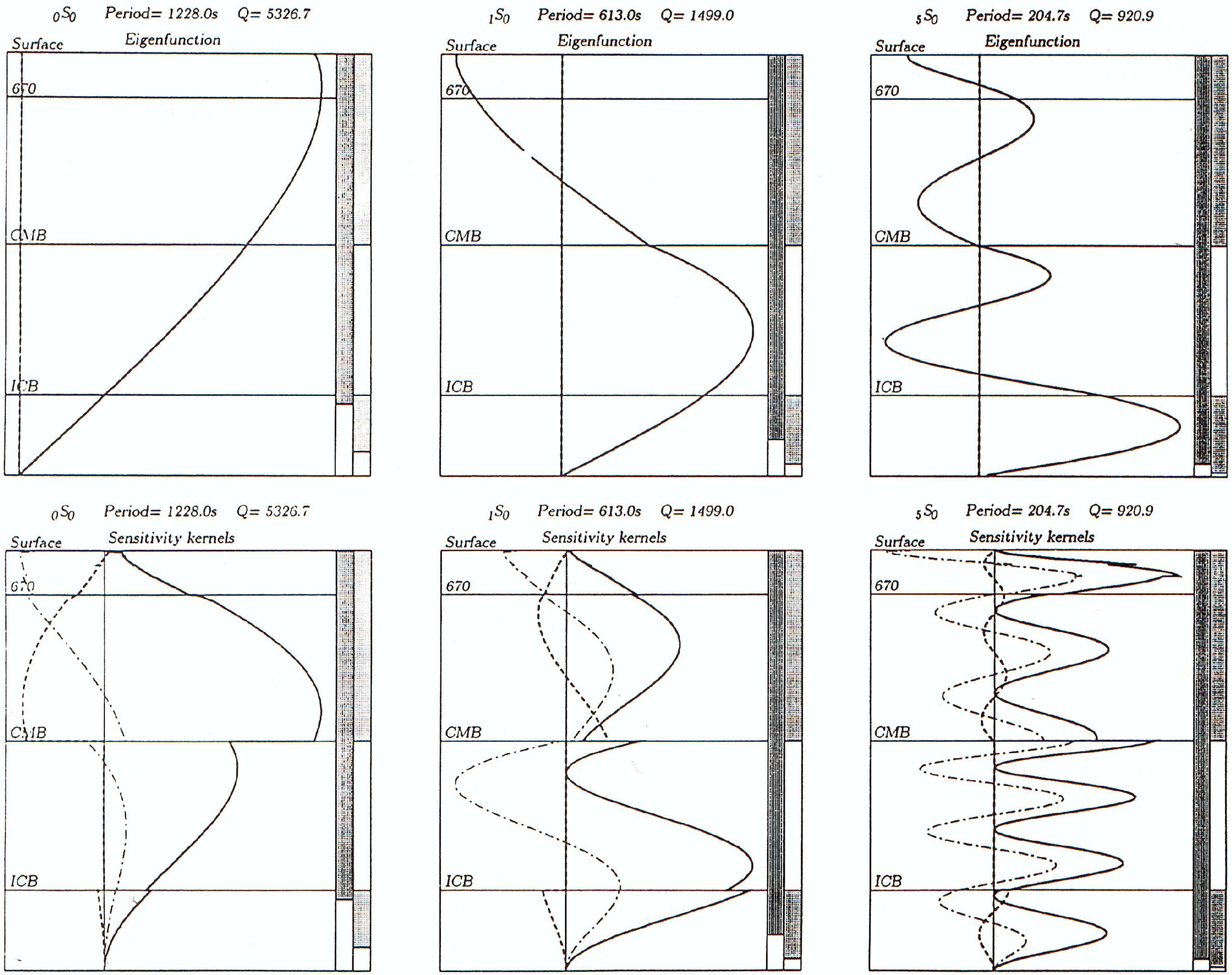

$_0S_0$ Period= 1228.0s Q= 5326.7
Surface
Eigenfunction
670
CMB
ICB
$_1S_0$ Period= 613.0s Q= 1499.0
Surface
Eigenfunction
670
CMB
ICB
$_5S_0$ Period= 204.7s Q= 920.9
Surface
Eigenfunction
670
CMB
ICB
$_0S_0$ Period= 1228.0s Q= 5326.7
Surface
Sensitivity kernels
670
CMB
ICB
$_1S_0$ Period= 613.0s Q= 1499.0
Surface
Sensitivity kernels
670
CMB
ICB
$_5S_0$ Period= 204.7s Q= 920.9
Surface
Sensitivity kernels
670
CMB
ICB

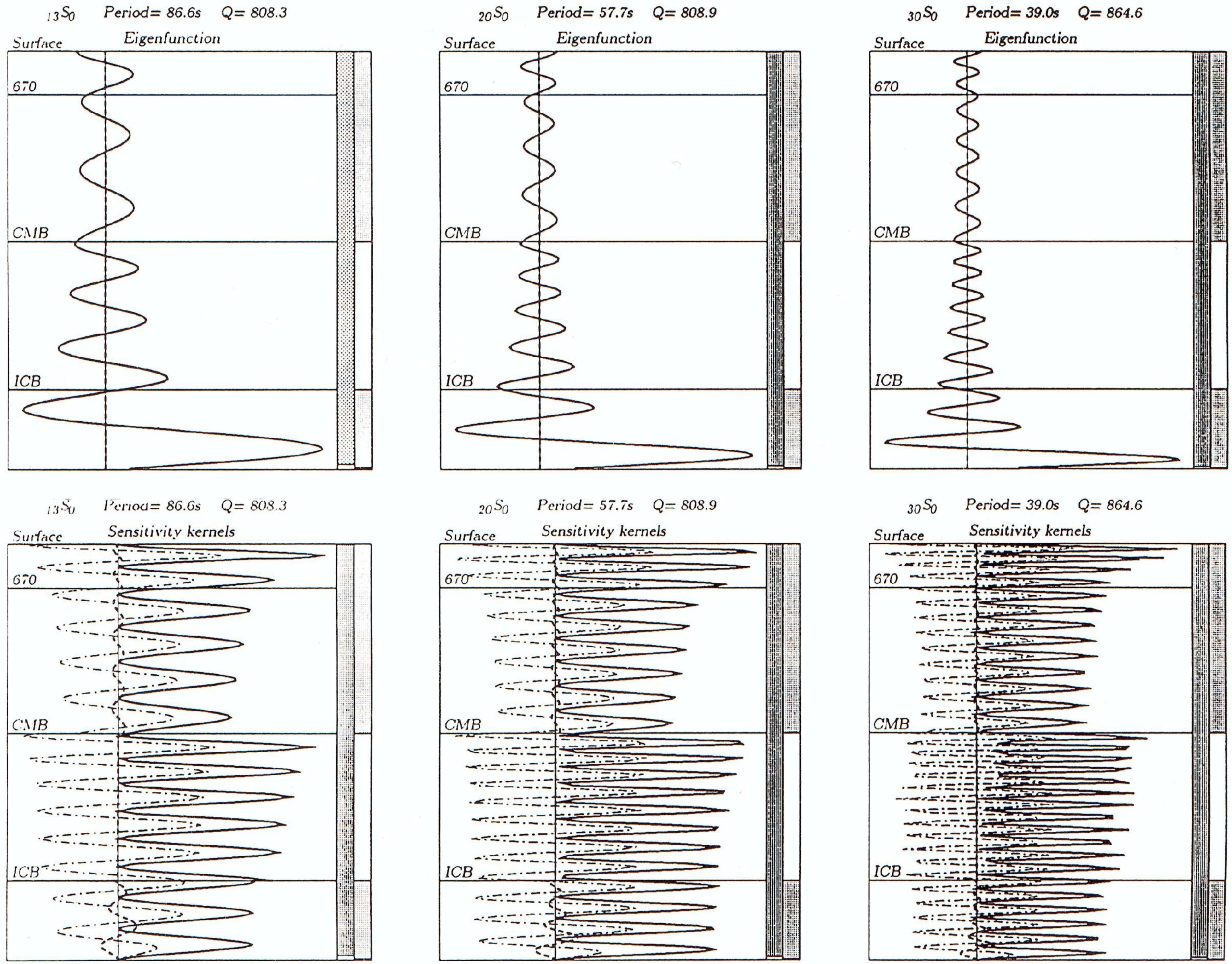

$_{13}S_0$ Period= 86.6s Q= 808.3
Surface Eigenfunction
670
CMB
ICB
$_{20}S_0$ Period= 57.7s Q= 808.9
Surface Eigenfunction
670
CMB
ICB
$_{30}S_0$ Period= 39.0s Q= 864.6
Surface Eigenfunction
670
CMB
ICB
$_{13}S_0$ Period= 86.6s Q= 808.3
Surface Sensitivity kernels
670
CMB
ICB
$_{20}S_0$ Period= 57.7s Q= 808.9
Surface Sensitivity kernels
670
CMB
ICB
$_{30}S_0$ Period= 39.0s Q= 864.6
Surface Sensitivity kernels
670
CMB
ICB